

# Current Biology

## Planar-Polarized Semaphorin-5c and Plexin A Promote the Collective Migration of Epithelial Cells in *Drosophila*

### Highlights

- Semaphorin-5c and Plexin A promote the collective migration of epithelial cells
- Semaphorin-5c is at each cell's leading edge, and Plexin A is at the trailing edge
- Semaphorin-5c can signal across cell-cell boundaries to suppress protrusions
- Semaphorin-5c signals through Plexin A and also interacts with Lar

### Authors

Claire G. Stedden, William Menegas, Allison L. Zajac, Audrey M. Williams, Shouqiang Cheng, Engin Özkan, Sally Horne-Badovinac

### Correspondence

shorne@uchicago.edu

### In Brief

Stedden et al. examine how Semaphorin-5c and Plexin A promote epithelial migration in the context of the *Drosophila* egg chamber. They show that Semaphorin-5c is planar polarized across the epithelium at the leading edge of each cell and that it directs cell motility by acting within the migrating cohort, not the surrounding environment.



# Planar-Polarized Semaphorin-5c and Plexin A Promote the Collective Migration of Epithelial Cells in *Drosophila*

Claire G. Stedden,<sup>1,2</sup> William Menegas,<sup>2,4</sup> Allison L. Zajac,<sup>2</sup> Audrey M. Williams,<sup>2</sup> Shouqiang Cheng,<sup>3</sup> Engin Özkan,<sup>3</sup> and Sally Horne-Badovinac<sup>1,2,5,\*</sup>

<sup>1</sup>Committee on Development, Regeneration, and Stem Cell Biology, The University of Chicago, 920 East 58<sup>th</sup> Street, Chicago, IL 60637, USA

<sup>2</sup>Department of Molecular Genetics and Cell Biology, The University of Chicago, 920 East 58<sup>th</sup> Street, Chicago, IL 60637, USA

<sup>3</sup>Department of Biochemistry and Molecular Biology, The University of Chicago, 929 East 57<sup>th</sup> Street, Chicago, IL 60637, USA

<sup>4</sup>Present address: McGovern Institute for Brain Research, Massachusetts Institute of Technology, 43 Vassar Street, Office: 46-3133, Cambridge, MA 02139, USA

<sup>5</sup>Lead Contact

\*Correspondence: [shorne@uchicago.edu](mailto:shorne@uchicago.edu)  
<https://doi.org/10.1016/j.cub.2019.01.049>

## SUMMARY

Collective migration of epithelial cells is essential for morphogenesis, wound repair, and the spread of many cancers, yet how individual cells signal to one another to coordinate their movements is largely unknown. Here, we introduce a tissue-autonomous paradigm for semaphorin-based regulation of collective cell migration. Semaphorins typically regulate the motility of neuronal growth cones and other migrating cell types by acting as repulsive cues within the migratory environment. Studying the follicular epithelial cells of *Drosophila*, we discovered that the transmembrane semaphorin, Sema-5c, promotes collective cell migration by acting within the migrating cells themselves, not the surrounding environment. Sema-5c is planar polarized at the basal epithelial surface such that it is enriched at the leading edge of each cell. This location places it in a prime position to send a repulsive signal to the trailing edge of the cell ahead to communicate directional information between neighboring cells. Our data show that Sema-5c can signal across cell-cell boundaries to suppress protrusions in neighboring cells and that Plexin A is the receptor that transduces this signal. Finally, we present evidence that Sema-5c antagonizes the activity of Lar, another transmembrane guidance cue that operates along leading-trailing cell-cell interfaces in this tissue, via a mechanism that appears to be independent of Plexin A. Together, our results suggest that multiple transmembrane guidance cues can be deployed in a planar-polarized manner across an epithelium and work in concert to coordinate individual cell movements for collective migration.

## INTRODUCTION

Collective migration of epithelial cells underlies numerous tissue-remodeling events [1, 2]. In embryos, epithelial migration shapes

organs, including the mammary gland, vasculature, kidney, and eye [3–6]. In adults, it closes wounds in the skin and cornea and facilitates metastasis [7–9]. For epithelial cells to migrate collectively, each cell must coordinate its movements with those of its neighbors. It is likely that both mechanical and biochemical signals are used to achieve this goal [10]. To date, however, few biochemical signals have been identified.

The *Drosophila* egg chamber provides a tractable system in which to identify these coordinating biochemical signals and the principles underlying their activity [11]. Egg chambers are organ-like structures that will each develop into one egg (Figure 1A). They have an inner germ cell cluster surrounded by follicular epithelial cells (follicle cells), whose basal surfaces contact the basement membrane (BM) extracellular matrix (ECM) that ensheathes the organ. From the time an egg chamber forms through stage 8 of oogenesis, the follicle cells collectively migrate along the BM [12, 13]. This motion causes the egg chamber to rotate within the BM (Figure 1B) and helps to create the ellipsoid shape of the egg. Each migrating follicle cell extends leading edge protrusions and has a parallel array of stress fibers along its basal surface that mediates adhesion to the BM. These actin-based structures all align in the direction of tissue movement, revealing a high degree of coordination among the cells (Figure 1C).

The migration of the follicular epithelium requires the receptor protein tyrosine phosphatase (RPTP) Lar and the cadherin Fat2, which are planar polarized at the basal epithelial surface along leading-trailing cell-cell interfaces [14–17]. Lar localizes to each cell's leading edge, and Fat2 localizes to the trailing edge, allowing them to mediate signaling between the leading and trailing edges of neighboring cells [14]. Whether other signaling systems also operate along these critical cell-cell interfaces is unknown.

The semaphorins are a family of both secreted and membrane-associated proteins that activate plexin receptors [18, 19]. They were first identified as repulsive cues for axon guidance but also regulate the motility of other cell types, including collectively migrating neural crest and endothelial cells [20, 21]. Typically, the plexin is expressed by the migrating cells and the semaphorin is expressed by cells within the migratory environment. When a plexin-expressing cell encounters a source of



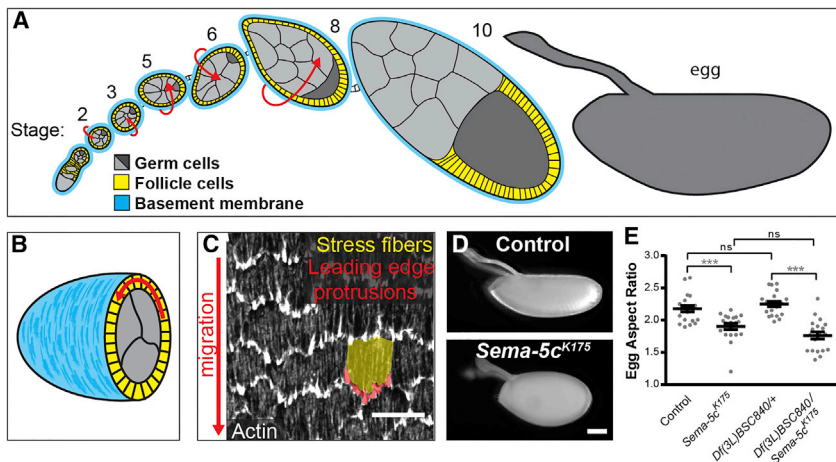


**Figure 1. Sema-5c Is Required for Egg Chamber Elongation**

(A) Illustration of a sagittal section through a developmental array of egg chambers. Arrows indicate rotation stages.

(B) Illustration of a transverse section through an egg chamber. Arrow indicates rotation.

(C) Image of the basal epithelial surface highlighting protrusions and stress fibers in one cell.

(D) Images of eggs from control and *Sema-5c*<sup>K175</sup> females.

(E) Quantification of egg aspect ratio. Eggs from *Sema-5c*<sup>K175</sup> females are rounder than controls.

Data in (E) represent mean  $\pm$  SEM. Unpaired t test. ns, not significant ( $p > 0.05$ ); \*\*\* $p < 0.001$ . Scale bars, 10  $\mu$ m (C) and 100  $\mu$ m (D). See also Figure S1.

semaphorin, it is repelled and thus confined to a particular migration path. *Drosophila* have three classes of semaphorins (Sema-1a/1b, Sema-2a/2b, and Sema-5c) and two plexins (PlexA and PlexB) [19]. It is conceivable that a transmembrane semaphorin and a plexin could be coexpressed within an epithelium, similar to Lar and Fat2, to allow each cell to influence the migratory behavior of its neighbors. However, no such signaling system involving a semaphorin has yet been found.

Here, we show that the transmembrane semaphorin, Sema-5c, functions within the follicle cells, not the migratory environment, to promote their collective motility. We further show that Sema-5c is planar polarized at the basal epithelial surface and enriched at each cell's leading edge. This location places it in a prime position to signal to the trailing edge of the cell ahead, which could coordinate migration direction between neighboring cells. Indeed, we find that Sema-5c can signal across cell-cell boundaries to suppress protrusions and that Plexin A appears to transduce this signal. Finally, we present evidence that Sema-5c also interacts with Lar. Altogether, these results show that diverse guidance cues can be deployed within an epithelium to coordinate cellular movements for collective motility.

## RESULTS

### Semaphorin-5c Is Required for Egg Chamber Elongation

We previously performed a genetic screen to identify genes required in the follicle cells to produce the elongated shape of the egg [22]. The *K175* allele found in this screen is homozygous viable. However, in homozygous females, the aspect ratio (length/width) of egg chambers and eggs is reduced (Figures 1D, 1E, and S1). Using deficiency mapping to identify the mutated gene, we found that females with *K175* *in trans* to *Df(3L)BSC840* produce rounded eggs similar to those of *K175* homozygotes (Figure 1E). This deficiency contains the *Semaphorin-5c* (*Sema-5c*) gene, which is non-essential for viability [23]. Sequencing *Sema-5c* coding regions in *K175* animals identified a point mutation, T393-to-A, which produces a premature stop codon near the protein's N terminus. Together, these data suggest that *K175* is a nonsense mutation in *Sema-5c* (*Sema-5c*<sup>K175</sup>) and that Sema-5c is required for egg chamber elongation.

### Loss of Semaphorin-5c Slows the Rate and Onset of Epithelial Migration

Defects in egg chamber elongation are often associated with impaired follicle cell migration [24], so we investigated whether Sema-5c is required for this process. *Ex vivo* live imaging showed that *Sema-5c* epithelia appear to be non-migratory (Figures 2A and 2B; Video S1). However, careful analysis of the actin cytoskeleton in fixed tissue, as discussed below, indicated that *Sema-5c* epithelia might have cryptic migratory ability.

The stress fibers at the basal surfaces of the follicle cells are aligned globally across the tissue, such that they all run parallel to the direction of movement [12, 25]. We quantify this global alignment with an order parameter, where zero represents no alignment and one represents perfect alignment. Global stress fiber alignment is high in wild-type epithelia when migration begins and increases until the end of migration at stage 8. By contrast, when migration is blocked, the alignment starts at the same high level but then decreases until the order parameter is near zero at stage 8 [12].

Because *ex vivo* live imaging revealed no obvious migration in *Sema-5c* epithelia, we expected to see a consistent decrease in global stress fiber alignment, similar to other non-migratory conditions. Instead, the alignment decreases until stage 5 but then recovers, such that many *Sema-5c* epithelia are indistinguishable from controls at stage 7 (Figures 2C and 2D). This observation suggested that *Sema-5c* epithelia might migrate extremely slowly and that the onset of motility might be delayed to stage 5-6. Given that *ex vivo* live imaging can only be performed for hours and follicle cell migration lasts  $\sim$ 2 days [11, 12], these subtle tissue dynamics could be missed by live imaging alone.

To test this, we developed an *in vivo* method to track epithelial migration over longer time periods, which leverages the fact that these cells secrete new matrix proteins into the BM as they migrate [13, 26]. We induced small clones of cells to express a monomeric red fluorescent protein (mRFP)-tagged version of the BM protein type IV collagen (Col IV-mRFP) and identified them by the fluorescent collagen within the secretory pathway of the expressing cells (Figure 3A). In a migratory epithelium, these clones deposit stripes of Col IV-mRFP into the BM behind them, creating a permanent record that migration occurred (Figures 3A-3E). By contrast, clones in a non-migratory *fat2*<sup>N103-2</sup> epithelium only deposit spots of Col IV-mRFP into the BM

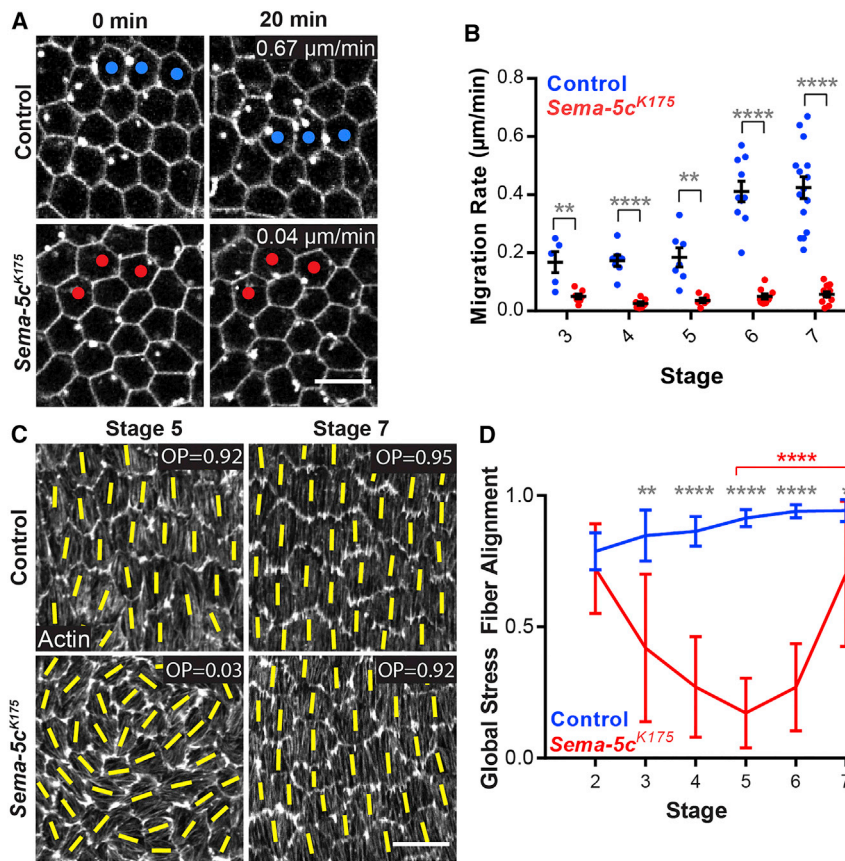


**Figure 2. Loss of Sema-5c Disrupts Epithelial Migration and Global Stress Fiber Alignment**

(A) Still images from videos of control and *Sema-5c<sup>K175</sup>* epithelia, stage 7. Dots mark the same cells over time.

(B) Quantification of migration rates for control and *Sema-5c<sup>K175</sup>* epithelia.

(C) Images of global stress fiber alignment in control and *Sema-5c<sup>K175</sup>* epithelia. Yellow lines show the primary stress fiber direction in each cell. OP, order parameter.

(D) Quantification of global stress fiber alignment in control and *Sema-5c<sup>K175</sup>* epithelia. Grey asterisks compare control to *Sema-5c<sup>K175</sup>*. Red asterisks compare *Sema-5c<sup>K175</sup>* stage 5 to stage 7.  $n \geq 8$  for all conditions.

Data represent mean  $\pm$  SEM in (B) and mean  $\pm$  SD in (D). Unpaired t test; \* $p < 0.05$ , \*\* $p < 0.01$ , \*\*\*\* $p < 0.0001$ . Scale bars, 10  $\mu$ m. See also [Video S1](#).

directly adjacent to the expressing cells (Figures 3F and 3G). We call the BM stripes COMETtails (clonal overexpression of matrix proteins for epithelial cell tracking). A similar method was recently published [27].

Using COMETtails, we found that *Sema-5c* epithelia display a phenotype that is intermediate between control and *fat2<sup>N103-2</sup>* epithelia. At stage 7, when global stress fiber alignment has largely recovered, all egg chambers have COMETtails (Figures 3I and 3J), which indicates that these *Sema-5c* epithelia do migrate. However, because *Sema-5c* COMETtails are shorter than controls and *ex vivo* live imaging reveals almost no movement (Figure 2B), the migration must be extremely slow. At stage 5, when stress fibers are maximally mis-aligned, only 25% of *Sema-5c* epithelia have COMETtails (Figures 3H and 3J). This observation is consistent with migration initiating in the majority of *Sema-5c* epithelia around stage 5–6. Altogether, these data show that loss of *Sema-5c* slows the rate of epithelial migration and often delays its onset.

### Semaphorin-5c Localizes to Each Cell's Leading Edge

To explore how *Sema-5c* promotes epithelial migration, we determined its localization in the egg chamber. We used the CRISPR-Cas9 system to insert three copies of GFP into the *Sema-5c* locus (*Sema-5c-3xGFP*). The resulting C-terminal protein fusion appears to be functional, as eggs from *Sema-5c-3xGFP* females elongate normally (Figure S2A). *Sema-5c-3xGFP* is expressed strongly in the follicle cells through stage 7, with little signal in the germ cells (Figure 4A). Optical sections

through the epithelium reveal that *Sema-5c-3xGFP* is on apical and lateral cell membranes and intracellular puncta that may represent endosomes (Figure 4B).

Because the migration machinery is at the tissue's basal surface, we were particularly interested in *Sema-5c*'s localization along this plane. We found that *Sema-5c-3xGFP* is both punctate and planar polarized along leading-trailing cell-cell interfaces (Figures 4C–4F). To determine

whether this localization corresponds to the leading edge, trailing edge, or both, we generated mosaic epithelia wherein some cells express *Sema-5c-3xGFP* and the remainder express untagged *Sema-5c*. Using leading edge protrusions to indicate migration direction, we found that *Sema-5c-3xGFP*-expressing cells migrating directly behind unmarked cells have GFP at their leading edges, whereas *Sema-5c-3xGFP*-expressing cells migrating directly ahead of unmarked cells largely lack GFP at their trailing edges (Figures 4G–4I, S2B, and S2C). Hence, *Sema-5c* is enriched at each cell's leading edge.

### Semaphorin-5c Can Suppress Protrusions in Neighboring Cells

One way that semaphorins regulate cell motility is by signaling non-cell-autonomously to suppress protrusions [28]. This activity was first identified in axon guidance, where semaphorins “collapse” the protrusive growth cone that pioneers the migration of an axon toward its target, but it also applies to other migratory cell types [29–31]. Although the level and location of protrusions appear normal in *Sema-5c* clones at stage 7 (Figure S2D), there is an abundance of mis-oriented protrusions in *Sema-5c* epithelia at stage 6 (Figures S2E–S2L). Moreover, the presence of short COMETtails in *Sema-5c* epithelia at this stage indicates that the mis-oriented protrusions can occur in conjunction with the early stages of epithelial motility. Together with the localization data above, these observations suggest that *Sema-5c* might signal from each cell's leading edge to regulate the site of protrusion formation in the cell ahead.

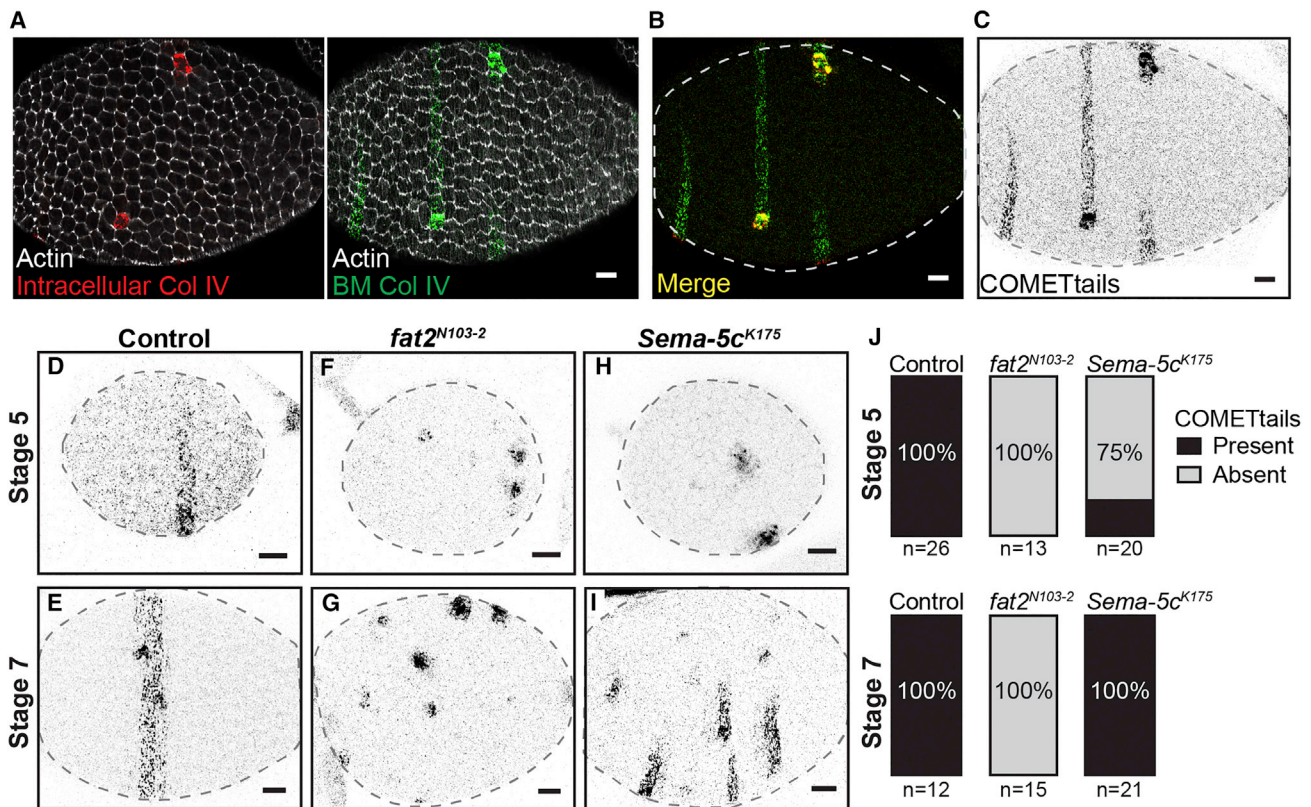


### Figure 3. Loss of Sema-5c Slows the Onset and Rate of Epithelial Migration

(A–C) The COMETtail method. (A) Clones expressing Col IV-mRFP are detected by the intracellular signal. Clones deposit stripes of Col IV-mRFP into the BM as they migrate (false-colored green). (B) Overlay of Col IV-mRFP images in (A). (C) Image from (B) in grayscale.

(D–I) Images of COMETtails from control (D and E), non-migratory *fat2<sup>N103-2</sup>* (F and G), and *Sema-5c<sup>K175</sup>* (H and I) epithelia.

(J) Quantification of COMETtail data. n, number of egg chambers examined.

Scale bars, 10  $\mu$ m.

To examine whether Sema-5c can suppress protrusions in neighboring cells, we overexpressed *Sema-5c* (*UAS-Sema-5c-GFP*) in follicle cell clones, which causes Sema-5c's localization to expand to the trailing edge (Figure S3A). In this overexpression condition, Sema-5c signals non-cell-autonomously to suppress leading edge protrusions in the cells directly behind the overexpressing cells (Figures 4J and 4K). The leading edge localization of the actin assembly factor SCAR is also reduced (Figures S3B and S3C). These phenotypes are only seen along cellular interfaces that directly contact the overexpressing cell, denoting an extremely short-range signal. Although Sema-5c is not normally localized to the trailing edge, this overexpression system demonstrates that Sema-5c can suppress protrusions and that it does so by signaling across cell-cell boundaries.

### Plexin A Mediates Semaphorin-5c Signaling

Our data suggest that Sema-5c promotes epithelial migration via intercellular signaling. To identify Sema-5c's receptor, we expressed RNAi against the *Drosophila* plexins. Two *PlexB* RNAi transgenes, previously validated in other tissues, do not affect egg elongation (Figure S4A). By contrast, two independent *PlexA* RNAi transgenes strongly deplete PlexA from the follicle cells and produce round eggs (Figures 5A, S4B, and S4C). Moreover,

global stress fiber alignment in *PlexA*-RNAi epithelia decreases until stage 5 but then recovers through stage 7, and we detected no obvious migration in *PlexA* RNAi epithelia by *ex vivo* live imaging (Figures 5B–5D; Video S2). Thus, depletion of PlexA causes migration-associated phenotypes that are strikingly similar to those caused by loss of Sema-5c.

We then mapped PlexA's localization pattern. Using both a bacterial artificial chromosome (BAC) transgene wherein *PlexA* is tagged with *myc* (*BAC-PlexA-myc*) and a PlexA antibody, we found that PlexA is punctate at the basal epithelial surface and planar polarized along leading-trailing cell-cell interfaces (Figures 5E and S4D). To determine PlexA's subcellular localization, we then used a mosaic method similar to that described for Sema-5c above (STAR Methods). This experiment revealed that, although some PlexA is at the leading edge, most PlexA is at the trailing edge (Figures 5F–5H and S4E–S4G). Thus, PlexA is in the right position to receive a Sema-5c signal from the leading edge of the cell behind.

To determine whether PlexA binds to Sema-5c, we probed their interaction *in vitro* and *in vivo*. First, we employed an ELISA-type assay using the ectodomains of PlexA and the five *Drosophila* semaphorins (Figures S5A and S5B). This assay revealed robust binding between PlexA and Sema-5c. Additionally, PlexA binds to its known ligands, Sema-1a and 1b [32],

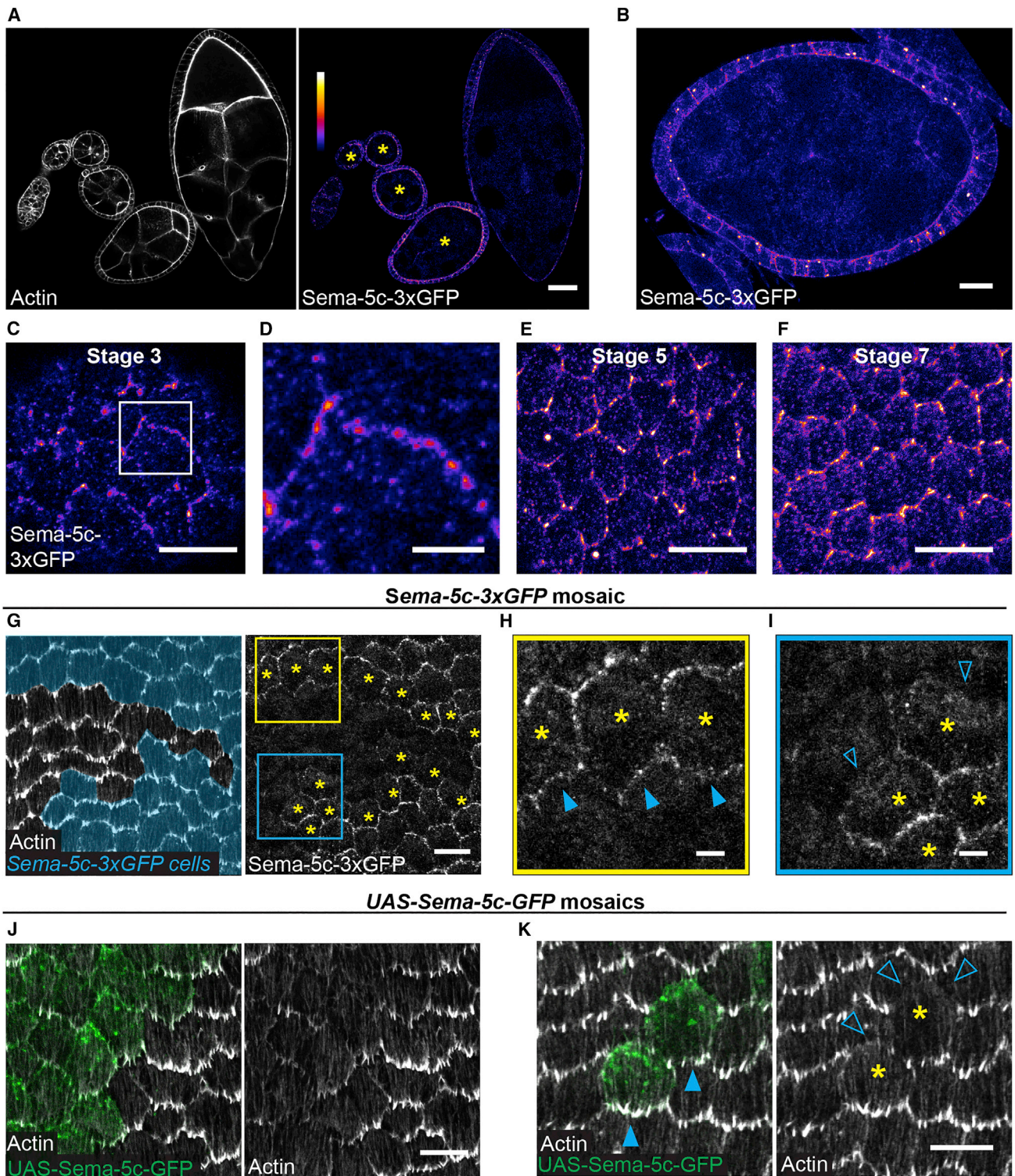


**Figure 4. Sema-5c Localizes to the Leading Edge and Can Suppress Protrusions in Neighboring Cells**

(A) Images of a sagittal section through an ovariolar expressing Sema-5c-3xGFP. Asterisks mark migratory stages. Heatmap index applies to (A)–(F).

(B) Image of a sagittal section through an egg chamber, stage 6. Sema-5c-3xGFP is on apical and lateral cell membranes and intracellular puncta.

(C–F) Images of the basal epithelial surface at stages 3 (C and D), 5 (E), and 7 (F). Sema-5c-3xGFP is punctate along leading-trailing cell-cell interfaces. (D) shows a zoom of the boxed region in (C).

(G–I) Images of the basal surface of a Sema-5c-3xGFP mosaic epithelium, stage 7.

(legend continued on next page)

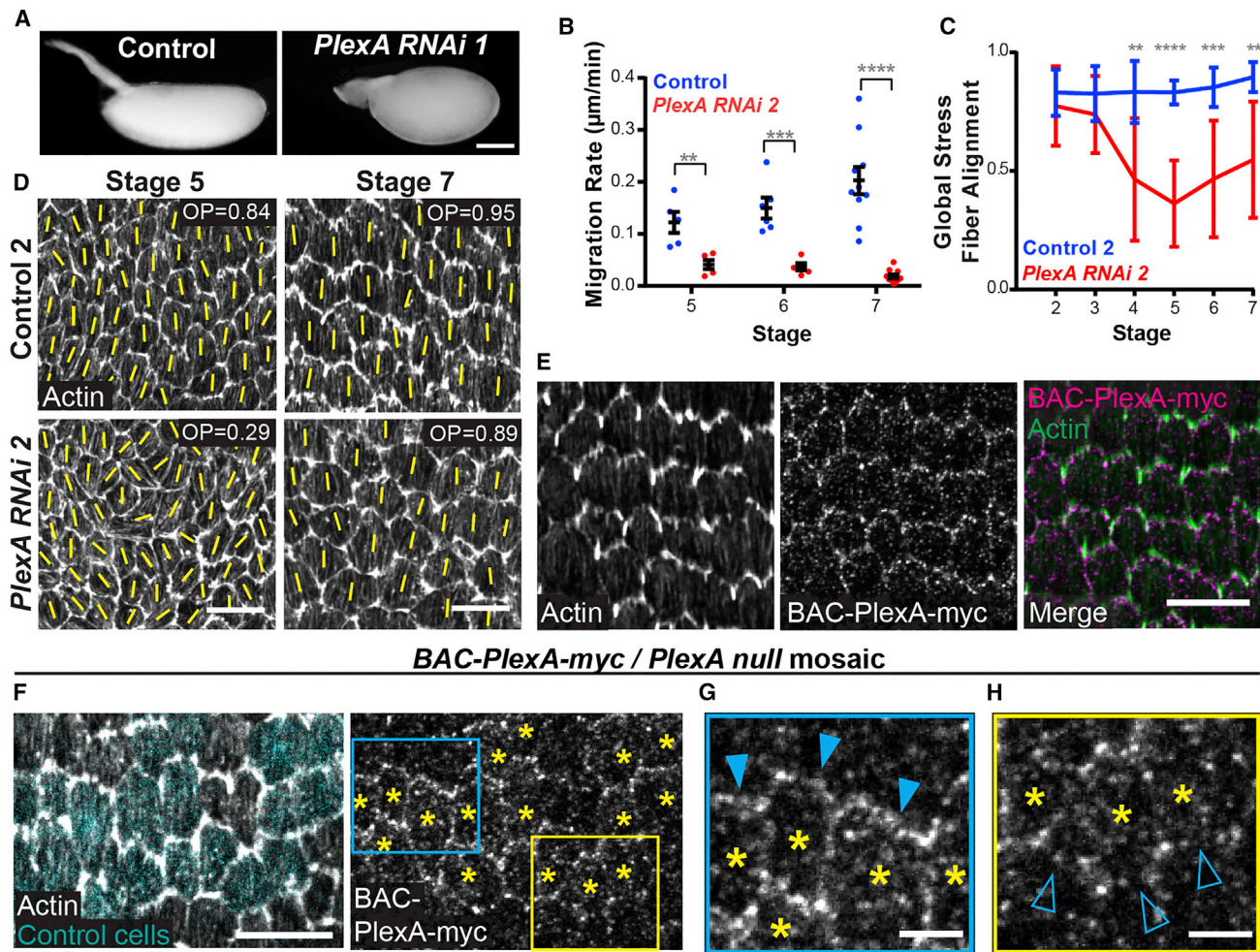


**Figure 5. Loss of PlexA Phenocopies Loss of Sema-5c, and PlexA Is Enriched at the Trailing Edge**

(A) Images of eggs from a control female and a female expressing *PlexA RNAi* in the follicular epithelium.

(B) Quantification of migration rates from control and *PlexA RNAi* epithelia.

(C) Quantification of global stress fiber alignment in control and *PlexA RNAi* epithelia.  $n \geq 8$  for all conditions.

(D) Images of global stress fiber alignment in control and *PlexA RNAi* epithelia. Yellow lines show the primary stress fiber direction in each cell. OP, order parameter.

(E) Images of the basal surface of a *BAC-PlexA-myc* epithelium, myc immunostaining, stage 7. PlexA is punctate along leading-trailing cell-cell interfaces.

(F–H) Images of the basal surface of a mosaic epithelium with *BAC-PlexA-myc* clones in a *PlexA*-null background, PlexA and myc immunostaining, stage 7. Asterisks mark cells expressing *BAC-PlexA-myc* at the clone boundary. (F) Control cells are marked in cyan. (G) Zoom of the blue boxed region in (F). *BAC-PlexA-myc*-expressing cells primarily have PlexA enriched at their trailing edge (solid triangles). (H) Zoom of the yellow boxed region in (F). *BAC-PlexA-myc*-expressing cells also have some PlexA at their leading edge (open triangles).

Data represent mean  $\pm$  SEM in (B) and mean  $\pm$  SD in (C). Unpaired t test; \*\* $p < 0.01$ , \*\*\* $p < 0.001$ , \*\*\*\* $p < 0.0001$ . Scale bars, 100  $\mu\text{m}$  (A), 10  $\mu\text{m}$  (D–F), and 3  $\mu\text{m}$  (G and H). See also [Figure S4](#) and [Video S2](#).

but not to Sema-2a and 2b, which are PlexB ligands [33, 34]. Second, we asked whether Sema-5c and PlexA are required for each other's localization. Although PlexA levels appear normal in *Sema-5c* epithelia (Figure S5C), Sema-5c-3xGFP is reduced at the basal surface of *PlexA-RNAi* epithelia (Figures

6A, 6B, and S5D). Despite this stabilizing effect of PlexA on Sema-5c, PlexA puncta are sparser and only sometimes colocalize with Sema-5c puncta (Figures 6C–6G) Altogether, these data indicate that PlexA and Sema-5c do interact but that their interaction *in vivo* may be transient.

(G) Cells expressing Sema-5c-3xGFP are pseudocolored cyan. Asterisks mark Sema-5c-3xGFP-expressing cells at the clone boundary. (H) Zoom of the yellow boxed region in (G). Sema-5c-3xGFP-expressing cells have GFP at their leading edge (solid triangles). (I) Zoom of the blue boxed region in (G). Sema-5c-3xGFP-expressing cells lack GFP at their trailing edge (open triangles).

(J and K) Images of the basal surface of *UAS-Sema-5c-GFP* mosaic epithelia, stage 7. (J) Protrusions are reduced in the clone. (K) Protrusions are present at the front of the clone (closed triangles) but are lost from cells directly behind the clone (open triangles). Asterisks mark the clone.

Scale bars, 100  $\mu\text{m}$  (A), 10  $\mu\text{m}$  (B, C, E–G, J, and K), and 3  $\mu\text{m}$  (D, H, and I). See also [Figures S2](#) and [S3](#).

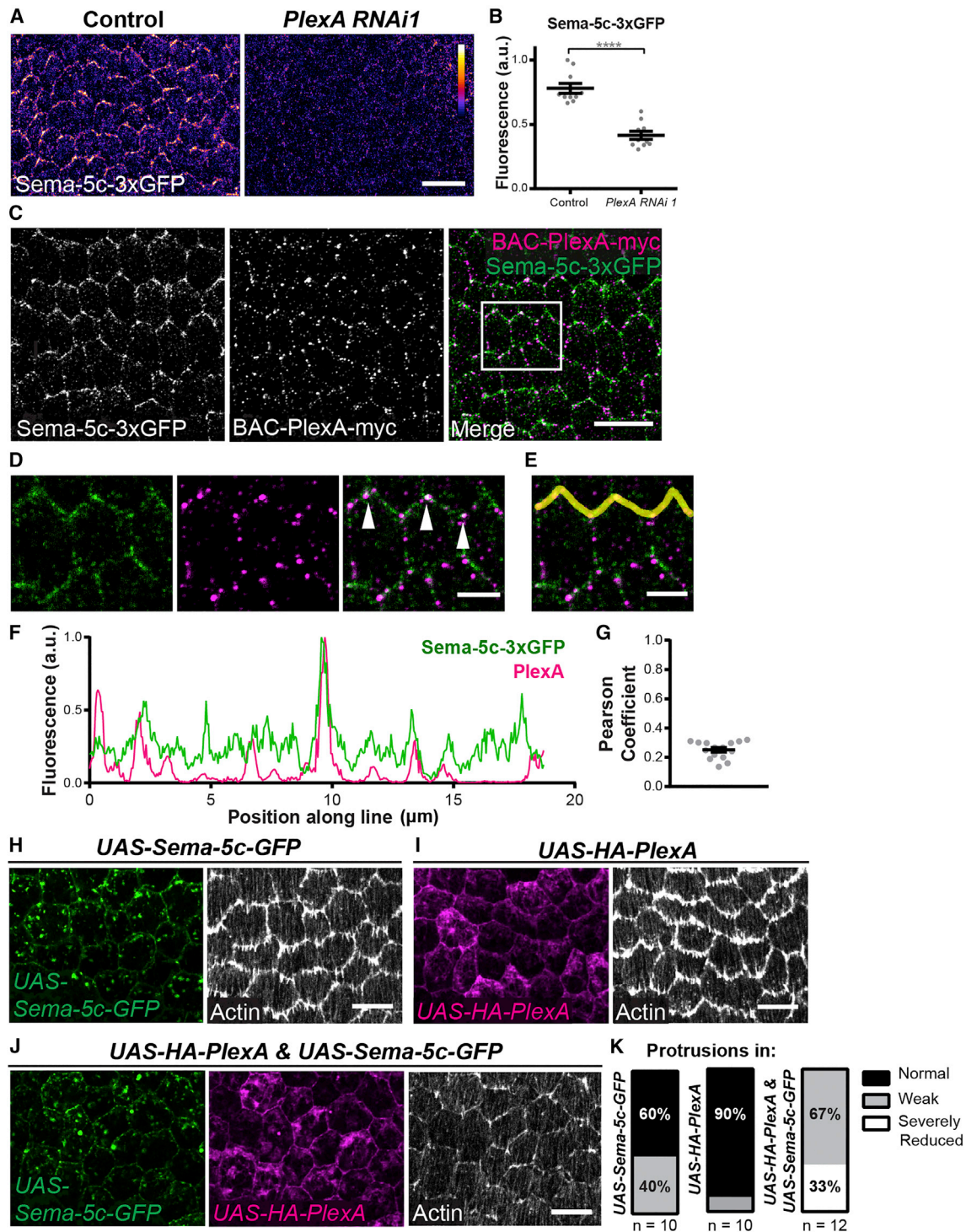


**Figure 6. PlexA Is the Likely Receptor for Sema-5c**

(A) Images of the basal epithelial surface, stage 7. *PlexA RNAi* reduces Sema-5c-3xGFP levels.

(B) Quantification of Sema-5c-3xGFP levels at cell-cell interfaces in control and *PlexA RNAi* epithelia, stage 7.

(C–E) Images of the basal surface of an epithelium expressing *Sema-5c-3xGFP* and *BAC-PlexA-myc*, myc immunostaining, stage 7 (C). (D and E) Zoom of boxed region in (C). White triangles indicate colocalization between Sema-5c and PlexA.

(F) Quantification of fluorescence intensities of Sema-5c-3xGFP and BAC-PlexA-myc along the cell-cell interfaces marked by the yellow line in (E).

(G) Pearson correlation coefficient for Sema-5c-3xGFP and BAC-PlexA-myc fluorescence intensities along leading-trailing cell-cell interfaces, stage 7. Each point is one epithelium in which a line scan was performed along 5–8 cell-cell interfaces.

(legend continued on next page)

Finally, we revisited our *Sema-5c* overexpression condition to ask whether PlexA mediates *Sema-5c*'s ability to suppress protrusions. Because there is some PlexA at each cell's leading edge, overexpressed *Sema-5c* may inhibit protrusions in the cell behind by signaling through this population of the receptor. Indeed, depleting PlexA from *UAS-Sema-5c-GFP* clones abrogates *Sema-5c*'s ability to suppress protrusions (Figures S5E–S5H), which shows that PlexA is required for *Sema-5c* activity. We further found that expressing either *UAS-HA-PlexA* or a low level of *UAS-Sema-5c-GFP* in the entire epithelium has only a minor effect on protrusions, whereas expressing both transgenes together strongly suppresses protrusions (Figures 6H–6K). Thus, overexpressed PlexA can also enhance *Sema-5c*'s ability to signal. Altogether, these data suggest that PlexA acts as a receptor for *Sema-5c* in the follicular epithelium.

### Semaphorin-5c Interacts with Lar

The localization patterns of *Sema-5c* and PlexA resemble those of Lar and Fat2, which suggests that these four proteins might work together to promote epithelial motility. However, neither *Sema-5c* clones (Figure S2D) nor *PlexA RNAi* clones (Figure S5F) show the defects in leading edge protrusions and/or trailing edge retraction caused by loss of Lar or Fat2 [14]. This observation argues against *Sema-5c* and PlexA being part of the Lar/Fat2 signaling system, yet there may still be crosstalk between the two pathways.

We therefore explored whether *Sema-5c*/PlexA and Lar/Fat2 interact at the genetic level. Removing one copy of *Lar* substantially rescues the egg shape defect in *Sema-5c* females (Figures 7A, S6A, and S6B). Reduced Lar dosage may allow migration to begin earlier in *Sema-5c* epithelia, as global stress fiber alignment is higher in the rescued epithelia than in *Sema-5c* epithelia (Figures 7B–7D and S6C). Reduced *Lar* dosage does not rescue the migration rate, however, as we detected no directional motility in rescued epithelia by *ex vivo* live imaging (Figure S6D). Removing one copy of *fat2* does not rescue the egg shape defect in *Sema-5c* females (Figure S6E), nor does removing one copy of *Lar* in *PlexA-RNAi* females (Figure S6F). Altogether, these data suggest that *Sema-5c* antagonizes Lar activity and that this interaction may be independent of Fat2 and PlexA.

Because *Sema-5c* and Lar both localize to the leading edge, we next asked whether they colocalize. The density of *Sema-5c* and Lar puncta is similar along the leading-trailing cell-cell interfaces, and they consistently overlap (Figures 7E–7I). Moreover, although Lar levels appear normal in *Sema-5c* and *PlexA RNAi* clones, *Sema-5c* levels are reduced in *Lar* clones (Figures 7J, S6G, and S6H). This reduction is not due to an effect on PlexA, as PlexA levels are normal in *Lar* clones (Figure S6I). Altogether, these data suggest that *Sema-5c* has a second function that involves a *cis* interaction with Lar.

## DISCUSSION

Here, we introduce a tissue-autonomous model for semaphorin signaling in collective cell migration (Figure 7K). Our data show

that *Sema-5c* acts as a migratory cue within the collectively migrating epithelial cells themselves instead of acting in the migratory environment. *Sema-5c* is planar polarized at the basal epithelial surface, localizing to each cell's leading edge. We envision that this placement allows *Sema-5c* to activate PlexA on the trailing edge of the cell ahead and thus communicate directional information between neighboring cells. We further identify an interaction between *Sema-5c* and Lar, which suggests that *Sema-5c* may play a second role in the Lar/Fat2 signaling pathway. Together, these results highlight how multiple guidance cues work in concert within an epithelium to coordinate cell movements for collective motility.

### Semaphorin-5c May Promote Collective Motility by Acting as a Repulsive Cue for Neighboring Cells

Given that overexpressing *Sema-5c* collapses protrusions in neighboring cells, we propose that *Sema-5c* may promote collective motility via contact inhibition of locomotion (CIL). CIL describes a set of behaviors exhibited by a migrating cell when it collides with another cell [35]. Specifically, the cell retracts its protrusions from the point of contact and repolarizes to migrate away in a new direction. CIL is mediated by signaling proteins on the cells' surfaces, including semaphorins and plexins [28, 36]. Although CIL is often used to disperse cells, cases exist where CIL appears to organize cells for collective movement [35]. We propose that the *Sema-5c* at each cell's leading edge could signal to suppress protrusions at the trailing edge of the cell ahead and thus direct the signal-receiving cell to polarize away from this point of contact such that both cells then migrate in the same direction. In this scenario, the semaphorin is a repulsive cue, similar to the most common function of semaphorins in axon guidance. Supporting this notion, we see an abundance of mis-oriented protrusions in *Sema-5c* epithelia at stage 6. Determining whether semaphorin-based CIL is operating in the follicular epithelium will be an important area for future work.

The role we have identified for *Sema-5c* in promoting collective migration may be conserved. *Sema-5c* is the only *Drosophila* semaphorin with direct orthologs in vertebrates (*Sema5A* and *Sema5B*). Moreover, similar to *Sema-5c*, the vertebrate class 5 semaphorins promote the migration of multiple cell types [30, 37–39] and can collapse protrusions non-cell-autonomously [30, 37]. Given that three of the five classes of vertebrate semaphorins are integral membrane proteins (classes 4–6), any one of these family members could promote collective migration similarly to *Sema-5c*, which opens the possibility that *Sema-5c*'s mechanism of action could be widely used.

### Semaphorin-5c Most Likely Signals through Plexin A

Four pieces of evidence suggest that PlexA is a *Sema-5c* receptor. First, the follicle cells require PlexA to migrate normally. Second, the dynamics of the global stress fiber pattern in *PlexA RNAi* epithelia is similar to that of *Sema-5c* epithelia. Third, PlexA and *Sema-5c* interact both *in vitro* and *in vivo*. Fourth, PlexA primarily localizes to each cell's trailing edge, placing it in the right position

(H–J) Coexpression of *PlexA* enhances the *Sema-5c* overexpression phenotype. Images are of the basal epithelial surface, stage 8. (H) A low level of *UAS-Sema-5c-GFP* mildly reduces protrusions. (I) *UAS-HA-PlexA* has little effect on protrusions. (J) Coexpressing both transgenes strongly reduces protrusions.

(K) Quantification of data in (H)–(J).

Data in (B) represent mean  $\pm$  SEM. Unpaired t test; \*\*\*\*p < 0.0001. Scale bars, 10  $\mu$ m (A, C, and H–J) and 3  $\mu$ m (D and E). See also Figure S5.



to receive a *Sema-5c* signal from the leading edge of the cell behind. This observation is particularly intriguing, as a vertebrate homolog of *PlexA*, *Plexin A1*, functions at the trailing edge of migrating dendritic cells [40].

Given that *PlexA* is required for *Sema-5c*'s localization, we were surprised to find that they only rarely colocalize. We are not aware of other studies that report colocalization of a semaphorin-plexin pair at the subcellular level, so the dynamics of the ligand-receptor interaction *in vivo* are mysterious. It is interesting to speculate that the repulsive nature of the semaphorin signal may necessitate a transient interaction with its receptor.

Although our data strongly suggest that *Sema-5c* signals through *PlexA*, more complex models are possible. For example, vertebrate class 5 semaphorins signal through both A- and B-type plexins [30, 37, 41, 42]. Thus, *Sema-5c* could also signal through *PlexB*. There may also be reverse signaling through *Sema-5c*'s intracellular domain [43]. Future work will determine whether these alternate modes of *Sema-5c* signaling also contribute to epithelial motility.

### Multiple Guidance Cues Work in Concert to Promote Epithelial Migration

The *Sema-5c/PlexA* and *Lar/Fat2* signaling systems both operate along leading-trailing cell-cell interfaces to promote collective motility. Although phenotypic differences argue against all four proteins acting in one pathway, three pieces of evidence indicate that *Sema-5c* interacts with *Lar*. First, *Sema-5c* and *Lar* colocalize at the basal epithelial surface. Second, *Lar* is required for *Sema-5c*'s localization. Third, reducing *Lar* dosage rescues the global stress fiber alignment and egg shape phenotypes caused by loss of *Sema-5c*. These data suggest that *Sema-5c* antagonizes *Lar* activity and further imply that *Lar* may inhibit cell migration under some circumstances. It is possible that *Sema-5c* plays two roles in the follicle cells—one with *PlexA* and one with *Lar*. Alternatively, the interaction between *Sema-5c* and *Lar* may represent a point of convergence between two otherwise separate signaling pathways.

Given that *Sema-5c* and *Lar* both localize to the leading edge, they most likely interact *in cis*. We envision two non-mutually exclusive models by which this could occur. Class 5 semaphorins and *Lar* both bind heparin sulfate proteoglycans [44, 45], making it possible that glycan chains could bridge an interaction between their ectodomains. Alternatively, the interaction could occur downstream of their intracellular domains [43]. A recent study showed that semaphorins interact with *Lar* family RPTPs in the nervous systems of *C. elegans* and mice [46]. However, the mechanism described therein is different, with *Lar* functioning *in cis* with the plexin to amplify a secreted semaphorin signal. Thus, there may be crosstalk between *Lar* and semaphorins in multiple contexts.

The protein families to which *Sema-5c*, *PlexA*, *Lar*, and *Fat2* belong are all known for their roles in nervous system development. Semaphorins and plexins are one of the canonical families of axon guidance cues [47], and *Lar* family RPTPs function in both axon guidance and synapse formation [48]. Although less

studied, Fat-like cadherins also help to wire the nervous system [49]. The steering of a growth cone toward its target represents a system in which a guidance cue from the cellular environment modulates the behavior of a migrating cell. We have now identified a situation wherein these same guidance cues are planar polarized across an epithelium to allow each cell within the tissue to modulate the migratory behavior of their neighbors for collective motility. A recent study noted that the appearance of the semaphorin and plexin families predates the evolution of the nervous system in metazoans [50]. The same is true for Fat-like cadherins [51]. Thus, the ancestral role for these guidance cues may be to regulate epithelial dynamics, with their role in guiding axons arising later.

### Collective Migration of the Follicle Cells Can Begin Late in Development from a Disordered State

Finally, this work elucidates the cellular parameters required for the follicular epithelium to migrate. The follicle cells typically begin migrating shortly after an egg chamber forms, and their stress fibers always show a high degree of global alignment [12]. We have discovered that neither of these features is strictly required for epithelial motility. Moreover, our observations that epithelial migration can begin later in development and can do so after the stress fiber pattern has become disordered, show that the ability of this epithelium to break symmetry and polarize is more robust than previously appreciated.

There is a *fat2* partial-loss-of-function condition that is phenotypically similar to *Sema-5c* [27, 52]. In this condition, epithelial migration is so slow that it cannot be detected by *ex vivo* live imaging. Moreover, migration is most likely delayed, as the global stress fiber pattern is disordered at stage 6 but recovers by stage 8. Future work will determine the extent to which these two mutant conditions phenocopy and whether these similarities indicate yet more points of convergence between the *Sema-5c/PlexA* and *Lar/Fat2* signaling systems.

The observation that some mutant epithelia polarize and begin migrating at stage 5-6 suggests that there may be developmentally programmed changes in the egg chamber that create a more favorable environment for epithelial motility. We previously noted that global stress fiber alignment and migration rate both increase in wild-type epithelia around this time [12]. This improved migratory ability could be due to higher BM stiffness, as stiffer matrices promote cell migration [53] and the stiffness of the follicular BM increases over time [54, 55]. Determining whether the cells are responding to mechanical changes in the BM, and how they do so, will be fertile areas for future research.

### Conclusions

This work introduces a tissue-autonomous role for semaphorins in guiding the collective migration of epithelial cells. Moreover, our observation that *Sema-5c* and *PlexA* act alongside *Lar* and *Fat2* to promote epithelial motility highlights the complex signaling interactions that occur along leading-trailing cell-cell interfaces to allow these cells to coordinate their individual movements for collective motility.

(J) Images of the basal surface of a *Lar*<sup>13.2</sup> mosaic epithelium, stage 7. *Sema-5c-3xGFP* is reduced in mutant cells.

(K) Illustration of our working model for *Sema-5c*'s role in follicle cell migration.

Data in (A) represent mean  $\pm$  SEM. Unpaired t test; ns, not significant ( $p > 0.05$ ); \*\*\*\* $p < 0.0001$ . Scale bars, 10  $\mu$ m (D, E, and J) and 3  $\mu$ m (F and G). See also Figure S6.

## STAR★METHODS

Detailed methods are provided in the online version of this paper and include the following:

- **KEY RESOURCES TABLE**
- **CONTACT FOR REAGENT AND RESOURCE SHARING**
- **EXPERIMENTAL MODEL AND SUBJECT DETAILS**
  - *Drosophila* genetics
- **METHOD DETAILS**
  - Time lapse video acquisition and microscopy
  - Fixed image acquisition and microscopy
  - Quantification of egg aspect ratio
  - Measurements of global stress fiber alignment
  - COMETtail analysis
  - *in vitro* binding assay
  - Quantification of protein localization
  - Quantification of protein colocalization
  - Quantification of protein levels
  - Quantification of protrusions
  - Generation of Sema-5c-3xGFP transgenic line
  - Generation of UAS-Sema-5c-GFP transgenic line
- **QUANTIFICATION AND STATISTICAL ANALYSIS**

## SUPPLEMENTAL INFORMATION

Supplemental Information can be found with this article online at <https://doi.org/10.1016/j.cub.2019.01.049>.

## ACKNOWLEDGMENTS

We thank Trudi Schüpbach, Allan Spradling, Jose Pastor-Pareja, Alex Koldkin, Johnathan Terman, David Van Vactor, and Takaki Komiyama for *Drosophila* stocks and reagents; Adam Isabella for illustrations and Python code; Maureen Cetera and Kari Barlan for experimental advice; and Darcy Andersen, Rich Wang, and Mitch Anderson for experimental assistance. Kristin Sherrard and Robert Carrillo provided valuable comments on the manuscript. Funding was provided by the following grants: NIH T32 GM007183 to C.G.S.; NIH T32 HD055164 to A.M.W.; American Heart Association 16POST2726018 and American Cancer Society 132123-PF-18-025-01-CSM postdoctoral fellowships to A.L.Z.; NIH R01 NS097161 and a Klingenstein-Simons Fellowship Award in the Neurosciences to E.Ö.; and American Cancer Society RSG-14-176 and NIH R01 GM126047 to S.H.-B.

## AUTHOR CONTRIBUTIONS

C.G.S., W.M., and S.H.-B. conceived the study. C.G.S. performed all experiments, including formal analysis and visualization, except the following: W.M. mapped the *Sema-5c* lesion and performed early phenotypic analysis; A.L.Z. created the *UAS-Sema-5c-GFP* line and assisted with design of the *Sema-5c-3xGFP* line; A.M.W. provided Figure 7J; and S.C. and E.Ö. provided Figures S5A and S5B. C.G.S. and S.H.-B. wrote the manuscript with editorial input from all other authors.

## DECLARATION OF INTERESTS

The authors declare no competing interests.

Received: July 4, 2018

Revised: December 14, 2018

Accepted: January 18, 2019

Published: February 28, 2019

## REFERENCES

1. Friedl, P., and Gilmour, D. (2009). Collective cell migration in morphogenesis, regeneration and cancer. *Nat. Rev. Mol. Cell Biol.* *10*, 445–457.
2. Mayor, R., and Etienne-Manneville, S. (2016). The front and rear of collective cell migration. *Nat. Rev. Mol. Cell Biol.* *17*, 97–109.
3. Ewald, A.J., Brenot, A., Duong, M., Chan, B.S., and Werb, Z. (2008). Collective epithelial migration and cell rearrangements drive mammary branching morphogenesis. *Dev. Cell* *14*, 570–581.
4. Michaelis, U.R. (2014). Mechanisms of endothelial cell migration. *Cell. Mol. Life Sci.* *71*, 4131–4148.
5. Sidhaye, J., and Norden, C. (2017). Concerted action of neuroepithelial basal shrinkage and active epithelial migration ensures efficient optic cup morphogenesis. *eLife* *6*, e22689.
6. Vasilyev, A., Liu, Y., Mudumana, S., Mangos, S., Lam, P.-Y., Majumdar, A., Zhao, J., Poon, K.-L., Kondrychyn, I., Korzh, V., and Drummond, I.A. (2009). Collective cell migration drives morphogenesis of the kidney nephron. *PLoS Biol.* *7*, e9.
7. Friedl, P., Locker, J., Sahai, E., and Segall, J.E. (2012). Classifying collective cancer cell invasion. *Nat. Cell Biol.* *14*, 777–783.
8. Liu, C.-Y., and Kao, W.W.-Y. (2015). Corneal epithelial wound healing. *Prog. Mol. Biol. Transl. Sci.* *134*, 61–71.
9. Shaw, T.J., and Martin, P. (2016). Wound repair: a showcase for cell plasticity and migration. *Curr. Opin. Cell Biol.* *42*, 29–37.
10. Ladoux, B., and Mège, R.-M. (2017). Mechanobiology of collective cell behaviours. *Nat. Rev. Mol. Cell Biol.* *18*, 743–757.
11. Horne-Badovinac, S., and Bilder, D. (2005). Mass transit: epithelial morphogenesis in the *Drosophila* egg chamber. *Dev. Dyn.* *232*, 559–574.
12. Cetera, M., Ramirez-San Juan, G.R., Oakes, P.W., Lewellyn, L., Fairchild, M.J., Tanentzapf, G., Gardel, M.L., and Horne-Badovinac, S. (2014). Epithelial rotation promotes the global alignment of contractile actin bundles during *Drosophila* egg chamber elongation. *Nat. Commun.* *5*, 5511.
13. Haigo, S.L., and Bilder, D. (2011). Global tissue revolutions in a morphogenetic movement controlling elongation. *Science* *331*, 1071–1074.
14. Barlan, K., Cetera, M., and Horne-Badovinac, S. (2017). Fat2 and Lar define a basally localized planar signaling system controlling collective cell migration. *Dev. Cell* *40*, 467–477.e5.
15. Bateman, J., Reddy, R.S., Saito, H., and Van Vactor, D. (2001). The receptor tyrosine phosphatase Dlar and integrins organize actin filaments in the *Drosophila* follicular epithelium. *Curr. Biol.* *11*, 1317–1327.
16. Viktorinová, I., König, T., Schlichting, K., and Dahmann, C. (2009). The cadherin Fat2 is required for planar cell polarity in the *Drosophila* ovary. *Development* *136*, 4123–4132.
17. Viktorinová, I., and Dahmann, C. (2013). Microtubule polarity predicts direction of egg chamber rotation in *Drosophila*. *Curr. Biol.* *23*, 1472–1477.
18. Jongbloets, B.C., and Pasterkamp, R.J. (2014). Semaphorin signalling during development. *Development* *141*, 3292–3297.
19. Yazdani, U., and Terman, J.R. (2006). The semaphorins. *Genome Biol.* *7*, 211.
20. Gu, C., and Giraudo, E. (2013). The role of semaphorins and their receptors in vascular development and cancer. *Exp. Cell Res.* *319*, 1306–1316.
21. Theveneau, E., and Mayor, R. (2012). Neural crest migration: interplay between chemorepellents, chemoattractants, contact inhibition, epithelial-mesenchymal transition, and collective cell migration. *Wiley Interdiscip. Rev. Dev. Biol.* *1*, 435–445.
22. Horne-Badovinac, S., Hill, J., Gerlach, G., 2nd, Menegas, W., and Bilder, D. (2012). A screen for round egg mutants in *Drosophila* identifies tricorned, furry, and misshapen as regulators of egg chamber elongation. *G3 (Bethesda)* *2*, 371–378.
23. Bahri, S.M., Chia, W., and Yang, X. (2001). Characterization and mutant analysis of the *Drosophila* *sema 5c* gene. *Dev. Dyn.* *221*, 322–330.
24. Cetera, M., and Horne-Badovinac, S. (2015). Round and round gets you somewhere: collective cell migration and planar polarity in elongating *Drosophila* egg chambers. *Curr. Opin. Genet. Dev.* *32*, 10–15.

25. Gutzeit, H.O. (1990). The microfilament pattern in the somatic follicle cells of mid-vitellogenic ovarian follicles of *Drosophila*. *Eur. J. Cell Biol.* 53, 349–356.
26. Isabella, A.J., and Horne-Badovinac, S. (2016). Rab10-mediated secretion synergizes with tissue movement to build a polarized basement membrane architecture for organ morphogenesis. *Dev. Cell* 38, 47–60.
27. Chen, D.-Y., Crest, J., and Bilder, D. (2017). A cell migration tracking tool supports coupling of tissue rotation to elongation. *Cell Rep.* 21, 559–569.
28. Hung, R.-J., and Terman, J.R. (2011). Extracellular inhibitors, repellents, and semaphorin/plexin/MICAL-mediated actin filament disassembly. *Cytoskeleton (Hoboken)* 68, 415–433.
29. Barberis, D., Artigiani, S., Casazza, A., Corso, S., Giordano, S., Love, C.A., Jones, E.Y., Comoglio, P.M., and Tamagnone, L. (2004). Plexin signaling hampers integrin-based adhesion, leading to Rho-kinase independent cell rounding, and inhibiting lamellipodia extension and cell motility. *FASEB J.* 18, 592–594.
30. Li, X., and Lee, A.Y.W. (2010). Semaphorin 5A and plexin-B3 inhibit human glioma cell motility through RhoGDIalpha-mediated inactivation of Rac1 GTPase. *J. Biol. Chem.* 285, 32436–32445.
31. van Rijn, A., Paulis, L., te Riet, J., Vasaturo, A., Reinieren-Beeren, I., van der Schaaf, A., Kuipers, A.J., Schulte, L.P., Jongbloets, B.C., Pasterkamp, R.J., et al. (2016). Semaphorin 7A promotes chemokine-driven dendritic cell migration. *J. Immunol.* 196, 459–468.
32. Winberg, M.L., Noordermeer, J.N., Tamagnone, L., Comoglio, P.M., Spriggs, M.K., Tessier-Lavigne, M., and Goodman, C.S. (1998). Plexin A is a neuronal semaphorin receptor that controls axon guidance. *Cell* 95, 903–916.
33. Ayoob, J.C., Terman, J.R., and Kolodkin, A.L. (2006). *Drosophila* Plexin B is a Sema-2a receptor required for axon guidance. *Development* 133, 2125–2135.
34. Wu, Z., Sweeney, L.B., Ayoob, J.C., Chak, K., Andreone, B.J., Ohyama, T., Kerr, R., Luo, L., Zlatic, M., and Kolodkin, A.L. (2011). A combinatorial semaphorin code instructs the initial steps of sensory circuit assembly in the *Drosophila* CNS. *Neuron* 70, 281–298.
35. Stramer, B., and Mayor, R. (2016). Mechanisms and in vivo functions of contact inhibition of locomotion. *Nat. Rev. Mol. Cell Biol.* 18, 43–55.
36. Deb Roy, A., Yin, T., Choudhary, S., Rodionov, V., Pilbeam, C.C., and Wu, Y.I. (2017). Optogenetic activation of Plexin-B1 reveals contact repulsion between osteoclasts and osteoblasts. *Nat. Commun.* 8, 15831.
37. Artigiani, S., Conrotto, P., Fazzari, P., Gilestro, G.F., Barberis, D., Giordano, S., Comoglio, P.M., and Tamagnone, L. (2004). Plexin-B3 is a functional receptor for semaphorin 5A. *EMBO Rep.* 5, 710–714.
38. Li, X., Law, J.W.S., and Lee, A.Y.W. (2012). Semaphorin 5A and plexin-B3 regulate human glioma cell motility and morphology through Rac1 and the actin cytoskeleton. *Oncogene* 31, 595–610.
39. Sadanandam, A., Rosenbaugh, E.G., Singh, S., Varney, M., and Singh, R.K. (2010). Semaphorin 5A promotes angiogenesis by increasing endothelial cell proliferation, migration, and decreasing apoptosis. *Microvasc. Res.* 79, 1–9.
40. Takamatsu, H., Takegahara, N., Nakagawa, Y., Tomura, M., Taniguchi, M., Friedel, R.H., Rayburn, H., Tessier-Lavigne, M., Yoshida, Y., Okuno, T., et al. (2010). Semaphorins guide the entry of dendritic cells into the lymphatics by activating myosin II. *Nat. Immunol.* 11, 594–600.
41. Duan, Y., Wang, S.H., Song, J., Mironova, Y., Ming, G.L., Kolodkin, A.L., and Giger, R.J. (2014). Semaphorin 5A inhibits synaptogenesis in early postnatal- and adult-born hippocampal dentate granule cells. *eLife* 3, e04390.
42. Matsuoka, R.L., Chivatakarn, O., Badea, T.C., Samuels, I.S., Cahill, H., Katayama, K., Kumar, S.R., Suto, F., Chédotal, A., Peachey, N.S., et al. (2011). Class 5 transmembrane semaphorins control selective Mammalian retinal lamination and function. *Neuron* 71, 460–473.
43. Battistini, C., and Tamagnone, L. (2016). Transmembrane semaphorins, forward and reverse signaling: have a look both ways. *Cell. Mol. Life Sci.* 73, 1609–1622.
44. Johnson, K.G., Tenney, A.P., Ghose, A., Duckworth, A.M., Higashi, M.E., Parfitt, K., Marcu, O., Heslip, T.R., Marsh, J.L., Schwarz, T.L., et al. (2006). The HSPGs Syndecan and Dallylike bind the receptor phosphatase LAR and exert distinct effects on synaptic development. *Neuron* 49, 517–531.
45. Kantor, D.B., Chivatakarn, O., Peer, K.L., Oster, S.F., Inatani, M., Hansen, M.J., Flanagan, J.G., Yamaguchi, Y., Sretavan, D.W., Giger, R.J., and Kolodkin, A.L. (2004). Semaphorin 5A is a bifunctional axon guidance cue regulated by heparan and chondroitin sulfate proteoglycans. *Neuron* 44, 961–975.
46. Nakamura, F., Okada, T., Shishikura, M., Uetani, N., Taniguchi, M., Yagi, T., Iwakura, Y., Ohshima, T., Goshima, Y., and Strittmatter, S.M. (2017). Protein tyrosine phosphatase  $\delta$  mediates the Sema3A-induced cortical basal dendritic arborization through the activation of Fyn tyrosine kinase. *J. Neurosci.* 37, 7125–7139.
47. Kolodkin, A.L., and Tessier-Lavigne, M. (2011). Mechanisms and molecules of neuronal wiring: a primer. *Cold Spring Harb. Perspect. Biol.* 3, a001727.
48. Han, K.A., Jeon, S., Um, J.W., and Ko, J. (2016). Emergent synapse organizers: LAR-RPTPs and their companions. In *International Review of Cell and Molecular Biology*, K.W. Jeon, ed. (Elsevier), pp. 39–65.
49. Avilés, E.C., and Goodrich, L.V. (2017). Configuring a robust nervous system with Fat cadherins. *Semin. Cell Dev. Biol.* 69, 91–101.
50. Yoo, S.K., Pascoe, H.G., Pereira, T., Kondo, S., Jacinto, A., Zhang, X., and Hariharan, I.K. (2016). Plexins function in epithelial repair in both *Drosophila* and zebrafish. *Nat. Commun.* 7, 12282.
51. Hulpiau, P., and van Roy, F. (2011). New insights into the evolution of metazoan cadherins. *Mol. Biol. Evol.* 28, 647–657.
52. Aurich, F., and Dahmann, C. (2016). A mutation in fat2 uncouples tissue elongation from global tissue rotation. *Cell Rep.* 14, 2503–2510.
53. Mason, B.N., Califano, J.P., and Reinhart-King, C.A. (2012). Matrix stiffness: a regulator of cellular behavior and tissue formation. In *Engineering Biomaterials for Regenerative Medicine*, S.K. Bhatia, ed. (Springer), pp. 19–37.
54. Chlasta, J., Milani, P., Runel, G., Duteyrat, J.-L., Arias, L., Lamiré, L.-A., Boudaoud, A., and Grammont, M. (2017). Variations in basement membrane mechanics are linked to epithelial morphogenesis. *Development* 144, 4350–4362.
55. Crest, J., Diz-Muñoz, A., Chen, D.-Y., Fletcher, D.A., and Bilder, D. (2017). Organ sculpting by patterned extracellular matrix stiffness. *eLife* 6, e24958.
56. Sweeney, L.B., Couto, A., Chou, Y.-H., Berdnik, D., Dickson, B.J., Luo, L., and Komiyama, T. (2007). Temporal target restriction of olfactory receptor neurons by Semaphorin-1a/PlexinA-mediated axon-axon interactions. *Neuron* 53, 185–200.
57. Zang, Y., Wan, M., Liu, M., Ke, H., Ma, S., Liu, L.P., Ni, J.Q., and Pastor-Pareja, J.C. (2015). Plasma membrane overgrowth causes fibrotic collagen accumulation and immune activation in *Drosophila* adipocytes. *eLife* 4, e07187.
58. Terman, J.R., Mao, T., Pasterkamp, R.J., Yu, H.-H., and Kolodkin, A.L. (2002). MICALs, a family of conserved flavoprotein oxidoreductases, function in plexin-mediated axonal repulsion. *Cell* 109, 887–900.
59. Frydman, H.M., and Spradling, A.C. (2001). The receptor-like tyrosine phosphatase lar is required for epithelial planar polarity and for axis determination within *drosophila* ovarian follicles. *Development* 128, 3209–3220.
60. Gratz, S.J., Cummings, A.M., Nguyen, J.N., Hamm, D.C., Donohue, L.K., Harrison, M.M., Wildonger, J., and O'Connor-Giles, K.M. (2013). Genome engineering of *Drosophila* with the CRISPR RNA-guided Cas9 nuclease. *Genetics* 194, 1029–1035.
61. Gratz, S.J., Ukken, F.P., Rubinstein, C.D., Thiede, G., Donohue, L.K., Cummings, A.M., and O'Connor-Giles, K.M. (2014). Highly specific and efficient CRISPR/Cas9-catalyzed homology-directed repair in *Drosophila*. *Genetics* 196, 961–971.
62. Schneider, C.A., Rasband, W.S., and Eliceiri, K.W. (2012). NIH Image to ImageJ: 25 years of image analysis. *Nat. Methods* 9, 671–675.

63. Schindelin, J., Arganda-Carreras, I., Frise, E., Kaynig, V., Longair, M., Pietzsch, T., Preibisch, S., Rueden, C., Saalfeld, S., Schmid, B., et al. (2012). Fiji: an open-source platform for biological-image analysis. *Nat. Methods* **9**, 676–682.
64. Aigouy, B., and Mirouse, V. (2013). ScientiFig: a tool to build publication-ready scientific figures. *Nat. Methods* **10**, 1048.
65. Rezakhaniha, R., Agianniotis, A., Schrauwen, J.T.C., Griffa, A., Sage, D., Bouten, C.V.C., van de Vosse, F.N., Unser, M., and Stergiopoulos, N. (2012). Experimental investigation of collagen waviness and orientation in the arterial adventitia using confocal laser scanning microscopy. *Biomech. Model. Mechanobiol.* **11**, 461–473.
66. Isabella, A.J., and Horne-Badovinac, S. (2015). Dynamic regulation of basement membrane protein levels promotes egg chamber elongation in *Drosophila*. *Dev. Biol.* **406**, 212–221.
67. Duffy, J.B., Harrison, D.A., and Perrimon, N. (1998). Identifying loci required for follicular patterning using directed mosaics. *Development* **125**, 2263–2271.
68. Meltzer, S., Yadav, S., Lee, J., Soba, P., Younger, S.H., Jin, P., Zhang, W., Parrish, J., Jan, L.Y., and Jan, Y.-N. (2016). Epidermis-derived semaphorin promotes dendrite self-avoidance by regulating dendrite-substrate adhesion in *Drosophila* sensory neurons. *Neuron* **89**, 741–755.
69. Pecot, M.Y., Tadros, W., Nern, A., Bader, M., Chen, Y., and Zipursky, S.L. (2013). Multiple interactions control synaptic layer specificity in the *Drosophila* visual system. *Neuron* **77**, 299–310.
70. Cetera, M., Lewellyn, L., and Horne-Badovinac, S. (2016). Cultivation and live imaging of *Drosophila* ovaries. *Methods Mol. Biol.* **1478**, 215–226.
71. Prasad, M., Jang, A.C.-C., Starz-Gaiano, M., Melani, M., and Montell, D.J. (2007). A protocol for culturing *Drosophila melanogaster* stage 9 egg chambers for live imaging. *Nat. Protoc.* **2**, 2467–2473.
72. Özkan, E., Carrillo, R.A., Eastman, C.L., Weiszmann, R., Waghray, D., Johnson, K.G., Zinn, K., Celniker, S.E., and Garcia, K.C. (2013). An extracellular interactome of immunoglobulin and LRR proteins reveals receptor-ligand networks. *Cell* **154**, 228–239.
73. Carrillo, R.A., Özkan, E., Menon, K.P., Nagarkar-Jaiswal, S., Lee, P.-T., Jeon, M., Birnbaum, M.E., Bellen, H.J., Garcia, K.C., and Zinn, K. (2015). Control of synaptic connectivity by a network of *Drosophila* IgSF cell surface proteins. *Cell* **163**, 1770–1782.

## STAR★METHODS

## KEY RESOURCES TABLE

REAGENT or RESOURCE	SOURCE	IDENTIFIER
<b>Antibodies</b>		
Mouse monoclonal anti-Lar	Developmental Studies Hybridoma Bank	9D82B3; RRID: AB_528202
Rabbit monoclonal anti-myc	Cell Signaling Technologies	71D10, #2278
Mouse monoclonal anti-SCAR	Developmental Studies Hybridoma Bank	P1C1; RRID: AB_2618386
Rabbit polyclonal anti-PlexA	Laboratory of Takaki Komiyama [56]	N/A
Mouse monoclonal anti- $\beta$ -Galactosidase	Promega	#Z378A; RRID: AB_430877
Rabbit polyclonal anti-HA	Rockland Inc.	#600-401-384; RRID: AB_218007
AlexaFluor-647, donkey anti-rabbit secondary	Invitrogen	#A31573; RRID: AB_2536183
AlexaFluor-647, donkey anti-mouse secondary	Invitrogen	#A31571; RRID: AB_162542
AlexaFluor-555, donkey anti-mouse secondary	Invitrogen	#A31570; RRID: AB_2536180
<b>Chemicals, Peptides, and Recombinant Proteins</b>		
Recombinant human insulin	Sigma	#I2643
CellMask Deep Red Plasma Membrane Stain	ThermoFisher	#C1006
Schneider's Drosophila medium	ThermoFisher	#21720-024
Fetal bovine serum	GIBCO	#10438-018
16% EM grade formaldehyde	Polysciences Inc	#18814-10
Slowfade antifade kit	ThermoFisher	#S2828
Fisherbrand cover glass 22 mm x 50 mm, No 1.5	Fisher	#12-544-D
Fisherbrand cover glass 22 mm x 22 mm, No 1.5	Fisher	#12-541-B
Premium microscope slides, frosted	Fisher	#12-544-3
Nail polish	Electron Microscopy Sciences	72180
Phalloidin-TRITC	Sigma	P1951
AlexaFluor-647 phalloidin	ThermoFisher	#A22287
Soda lime glass beads, 48-51 $\mu$ m	Cospheric LLC	S-SLGMS-2.5
DAPI	Sigma	D9542
<b>Experimental Models: Organisms/Strains</b>		
D. melanogaster. Standard control strain: w[1118]	Bloomington Drosophila Stock Center	BDSC: 3605; FlyBase ID: FBst0003605
D. melanogaster. traffic jam-Gal4: y* w*; P{w+mW.hs = GawB}NP1624/CyO, P{w- = UAS-lacZ.UW14}UW14	Kyoto Stock Center	DGRC: 104055
D. melanogaster. w; Sema-5c[K175], FRT80B	Laboratory of Sally Horne-Badovinac [22]	N/A
D. melanogaster. w[*]; P{ry[+t7.2] = neoFRT}80B ry[506]	Bloomington Drosophila Stock Center	BDSC: 1988; FlyBase ID: FBst0001988
D. melanogaster. w[1118]; Df(3L)BSC840, P+PBac{w[+mC] = XP3.RB5}BSC840/TM6C, Sb [1] cu [1]	Bloomington Drosophila Stock Center	BDSC: 29024; FlyBase ID: FBst0029024
D. melanogaster. P{UAS-Col4a1.RFP} [previously called UAS-CG25C-RFP]	Laboratory of Jose Pastor-Pareja [57]	FlyBase ID: FBtp0110407
D. melanogaster. w[*]; P{w[+mC] = AyGAL4}25, P{w[+mC] = UAS-EGFP}5a.2; P{w[+mC] = UAS-bnl.S}A1-1/TM6B, Tb [1]	Bloomington Drosophila Stock Center	BDSC: 64213; FlyBase ID: FBst0064231
D. melanogaster. y[1] w[*]; P{w[+mC] = AyGAL4}25 P{w[+mC] = UAS-lacZ.NZ}20b/CyO, y[+]	Bloomington Drosophila Stock Center	BDSC: 4410; FlyBase ID: FBst0004410
D. melanogaster. w[1118]; P{w[+mC] = AyGAL4}25/CyO	Bloomington Drosophila Stock Center	BDSC: 3953; FlyBase ID: FBst0003953
D. melanogaster. w[1118]; P{w[+mC] = UAS-Dcr-2.D}10	Bloomington Drosophila Stock Center	BDSC: 24651; FlyBase ID: FBst0024651

(Continued on next page)

**Continued**

REAGENT or RESOURCE	SOURCE	IDENTIFIER
D. melanogaster. W[1118]; P{w[+mC] = GAL4-Act5c(FRT.CD2).P}S, P{w[+mC] = UAS-RFP.W}3/TM3, Sb [1]	Bloomington Drosophila Stock Center	BDSC: 30558; FlyBase ID: FBst0030558
D. melanogaster. w;; Sema-5c-3xGFP	This paper	N/A
D. melanogaster. w;; Sema-5c-3xGFP, FRT80	This paper	N/A
D. melanogaster. w;; UAS-Sema-5c-GFP	This paper	N/A
D. melanogaster. w; UAS-Sema-5c-GFP	This paper	N/A
D. melanogaster. y[1] w[*]; P{w[+mW.hs] = en2.4-GAL4}e22c P{w[+mC] = UAS-FLP.D}JD1/CyO	Bloomington Drosophila Stock Center	BDSC: 5083; FlyBase ID: FBst0005083
D. melanogaster. y[1] w[1118]; P{w[+mC] = Ubi-mRFP.nls}2L P{ry[+t7.2] = neoFRT}40A/CyO	Bloomington Drosophila Stock Center	BDSC: 34500; FlyBase ID: FBst0034500
D. melanogaster. y[1] w[*]; P{w[+mW.hs] = GawB}T155 P{w[+mC] = UAS-FLP.D}JD2	Bloomington Drosophila Stock Center	BDSC: 5082; FlyBase ID: FBst0005082
D. melanogaster. w[*]; P{w[+mC] = Ubi- GFP.D}61EF P{ry[+t7.2] = neoFRT}80B	Bloomington Drosophila Stock Center	BDSC: 1620; FlyBase ID FBst0001620
D. melanogaster. RNAi of PlexA: w[1118]; P{GD14483}v27240/CyO	Vienna Drosophila Resource Center	VDRC ID: 27240
D. melanogaster. RNAi of PlexA: y[1] sc[*] v[1]; P{y[+t7.7] v[+t1.8] = TRiP.HM05221}attP2	Bloomington Drosophila Stock Center	BDSC: 30483; FlyBase ID: FBst0030483
D. melanogaster. RNAi of PlexB: w[1118]; P{GD14473}v27220	Vienna Drosophila Resource Center	VDRC ID: 27220
D. melanogaster. RNAi of PlexB: w[1118]; P{GD3150}v12167	Vienna Drosophila Resource Center	VDRC ID: 12167
D. melanogaster. BAC:PlexA-myc	Laboratory of Alex Kolodkin [50]	N/A
D. melanogaster. w[*]; Df(4)C3/In(4)ci[D], ci[D] pan[ciD] sv[spa-pol]	Bloomington Drosophila Stock Center	BDSC: 7083; FlyBase ID: FBst0007083
D. melanogaster. RNAi of RFP: y[1] sc[*] v[1]; P{y[+t7.7] v[+t1.8] = TRiP.HMS05713}attP40	Bloomington Drosophila Stock Center	BDSC: 67852; FlyBase ID: FBst0067852
D. melanogaster. UAS-HA-PlexA	Laboratory of Johnathan Terman [58]	N/A
D. melanogaster. w;; BAC-PlexA-myc, ubiGFP, h, FRT80B/TM6; Df(4)C3/ciD	Laboratory of Trudi Schüpach	N/A
D. melanogaster. yw hsFlp;; FRT80B, e ca/TM6; Df(4)C3/PlexA[MB09499]/ciD	Laboratory of Trudi Schüpach	N/A
D. melanogaster. Lar[Bola1]	Laboratory of Allan Spradling [59]	FlyBase ID: FBal0095667
D. melanogaster. Lar[Bola2]	Laboratory of Allan Spradling [59]	Flybase ID: Fbal0095666
D. melanogaster. w; Lar[13.2], FRT0A	Laboratory of David Van Vactor [15]	Flybase ID: FBst0008774
D. melanogaster. w;; fat2[N103-2], FRT80B	Laboratory of Sally Home-Badovinac [22]	FlyBase ID: Fbal0267777
D. melanogaster. P{ry[+t7.2] = hsFLP}22, w[*]	Bloomington Drosophila Stock Center	BDSC: 8862; FlyBase ID: FBst0008862
<b>Oligonucleotides</b>		
Primer for Sema-5c gRNA: 5'-GTTGCCTAGCGGGT CACGACCGG-3'	This paper	N/A
<b>Recombinant DNA</b>		
Plasmid: Sema-5c-3xGFP floxDsRed, See <a href="#">Methods S1</a>	This paper	N/A
Plasmid: p:U6:2 Sema-5c chiRNA, See <a href="#">Methods S1</a>	This paper	N/A
Plasmid: pU6-BbsI-chiRNA	[60]	N/A
Plasmid - 3xP3-RFP source: pHD-DsRed-attP	[61]	N/A
Plasmid - 3xGFP source: pmEGFP-13	Addgene	36410
Vector: pENTR/D-TOPO	Invitrogen	#K240020

(Continued on next page)

**Continued**

REAGENT or RESOURCE	SOURCE	IDENTIFIER
Drosophila Gateway Collection vector pTWG	Carnegie Institution for Science	<a href="https://emb.carnegiescience.edu/Drosophila-gateway-vector-collection">https://emb.carnegiescience.edu/Drosophila-gateway-vector-collection</a>
Sema-5c full length cDNA, Berkeley Drosophila Genome Project Gold Collection	Drosophila Genomics Resource Center	Clone ID: RE68041
Software and Algorithms		
ImageJ version 2.0.0	[62, 63]	<a href="https://fiji.sc/">https://fiji.sc/</a>
ScientiFig Plugin for ImageJ	[64]	<a href="https://grr.gred-clermont.fr/labmirouse/software/">https://grr.gred-clermont.fr/labmirouse/software/</a>
OrientationJ Plugin for ImageJ	[65]	<a href="http://bigwww.epfl.ch/demo/orientation/#soft">http://bigwww.epfl.ch/demo/orientation/#soft</a>
Prism Version 6.07 for Windows	GraphPad	N/A
Custom Python Script	[66]	N/A

**CONTACT FOR REAGENT AND RESOURCE SHARING**

Further information and requests for resources and reagents should be directed to and will be fulfilled by the Lead Contact, Sally Horne-Badovinac ([shorne@uchicago.edu](mailto:shorne@uchicago.edu)).

**EXPERIMENTAL MODEL AND SUBJECT DETAILS*****Drosophila* genetics**

*D. melanogaster* was cultured on cornmeal molasses agar food using standard techniques. All experiments were performed on adult females. For most experiments, crosses were raised at 25°C and experimental females were aged on yeast with males for 2-3 days at the same temperature. Experimental genotypes for each figure panel are in Table S1. The culturing conditions for the females in each experiment are detailed in Table S2.

Clones of either *Sema-5c*<sup>K175</sup> mutant cells or *Sema-5c-3xGFP* expressing cells were produced using *FRT80B* with *e22c-Gal4* driving *FLP* recombinase expression [67]. For Flip out clones, *UAS* lines were crossed to flies with *FLP* recombinase under a heat shock promoter and an *Act5c>>Gal4* Flip out cassette with or without *UAS-GFP* or *UAS-RFP*. Heat shock was induced by incubating pupae and adults at 37°C for 1 h, followed by 1 h of recovery at 25°C, and then another hour at 37°C. This heat shock procedure was performed 3 times over the course of 2 days. Females that eclosed during the period were placed on yeast with males overnight and dissected the next day.

For the studies of the Plexin receptors, the following RNAi lines were used: *UAS-PlexA-RNAi* 1 (v27240, GD14483), *UAS-PlexA-RNAi* 2 (TriP.HM05221), *UAS-PlexB-RNAi* 1 (v27220, GD14473), and *UAS-PlexB-RNAi* 2 (v12167, GD3150) [68].

Stocks are from Bloomington *Drosophila* Stock Center with the following exceptions. *UAS-PlexA-RNAi*<sup>GD14483</sup>, *UAS-PlexB-RNAi*<sup>GD14473</sup>, and *UAS-PlexB-RNAi*<sup>GD3150</sup> are from the Vienna *Drosophila* Resource Center. *Traffic jam-Gal4* (104055) is from the *Drosophila* Genetic Resource Center in Kyoto. *Lar<sup>Bola1</sup>* and *Lar<sup>Bola2</sup>* are a gift from Allan Spradling [59]. *UAS-Col4a1-mRFP* is a gift from Jose Pastor-Pareja [57]. *Lar<sup>13.2</sup>*, *FRT40A* is a gift from David Van Vactor [15]. The *BAC-PlexA-myc* strain is a gift from Alex Kolodkin [50, 69]. *UAS-HA-PlexA* is a gift from Johnathan Terman [58]. Both *w<sup>1118</sup>*; *BAC-PlexA-myc*, *ubi-GFP*, *h*, *FRT80B/TM6*; *Df(4)C3/CiD* and *yw*, *hsFLP*; *FRT80B*, *e*, *ca/TM6*; *PlexA<sup>MB</sup>/CiD* are gifts from Trudi Schüpbach. *Sema-5c*<sup>K175</sup> and *fat2*<sup>N103-2</sup> are from [22] and *Fat2-3xGFP* is from [14].

**METHOD DETAILS****Time lapse video acquisition and microscopy**

*Ex vivo* live imaging of egg chambers was performed largely as described [70, 71], with the exact procedure outlined below. Experimental females were collected 1-2 days after eclosion and aged on yeast for 2 days. Ovaries were dissected in live imaging media (Schneider's *Drosophila* medium containing 15% FBS and 200 µg/mL insulin) containing CellMask Deep Red Plasma Membrane Stain (Thermo-Fisher; 1:1000). After carefully removing the muscle sheaths with forceps, individual ovarioles were transferred to fresh live imaging media to wash out excess CellMask. The ovarioles and media were transferred to a glass slide; 51 µm Soda Lime Glass beads (Cospheric LLC) were added to support a 22 × 22 µm No. 1.5 coverslip. The edges of the coverslip were sealed with Vaseline to prevent evaporation. Each slide was used for no more than 2 h. All egg chambers were examined for damage prior to imaging, using CellMask to highlight damaged areas, as damaged egg chambers do not rotate. Egg chambers were imaged with one of two laser-scanning confocal microscopes running Zen 2.3 acquisition software, either a Zeiss LSM 800 with a 40x/1.3 NA EC Plan-NEOFLUAR objective, or a Zeiss LSM 880 with 40x/1.3 Plan-APOCHROMAT objective. Time-lapse movies were performed by capturing single confocal slices near the basal epithelial surface every 60 s. To calculate epithelial migration rates, kymographs

were generated from the time-lapse image stacks in Fiji (ImageJ) [62, 63] by drawing a single line across several cell diameters in the direction of migration. The migration rate for each epithelium was then determined by measuring the slope of 3–4 kymograph lines and averaging the values. Please see [14] for an illustration of this technique.

### Fixed image acquisition and microscopy

Ovaries were dissected in live imaging media, as described above. To isolate individual ovarioles, the muscle sheaths were either removed with forceps during dissection or by gentle pipetting post-fixation. In all cases, egg chambers at stage 10 or older were discarded. Egg chambers were fixed for 15 min in 4% EM grade formaldehyde (Polysciences) in PBT (PBS + 0.1% Triton X-100), the one exception is the use of 4% formaldehyde in Schneider's medium when immunostaining for Lar. To stain F-actin, egg chambers were washed 3x in PBT, incubated in TRITC Phalloidin (1:200 for 25 min, Sigma) or AlexaFluor-647 phalloidin (1:50 overnight or 1:30 for 3 h, Invitrogen), then washed 3x in PBT and mounted with one drop of SlowFade Antifade (Invitrogen) onto a slide with a 22 × 50mm No. 1.5 coverslip. For antibody staining, egg chambers were fixed as above, washed 4x in either PBT, PBT2 or PBT3 (PBS + 0.1%, 0.2% or 0.3% Triton X-100, respectively), and incubated at 4 °C overnight with the primary antibody. Then egg chambers were washed 4x, incubated with secondary antibodies conjugated to AlexaFluor-555, or –647 (Invitrogen, 1:200) for 2–3 h at room temperature, washed 4x and mounted as above. Anti-Lar (9D82B3, 1:200 concentrate) and anti-SCAR (P1C1, 1:200 concentrate) are from the Developmental Studies Hybridoma Bank, anti-β-Galactosidase is from Promega (Z378A, 1:200), anti-myc is from Cell Signaling Technologies (71D10, 1:200) and anti-HA is from Rockland Inc. (600-401-384, 1:250). Anti-PlexA is a gift from Takaki Komiyama [56], and was pre-absorbed overnight on egg chambers expressing *UAS-PlexA-RNAi* to reduce background signal prior to tissue staining and used at 1:1000. Tissue was imaged with one of the two scanning confocal microscopes described above, using the same objectives or a 63x/1.4 NA Plan-APOCHROMAT objective. For all images a single confocal slice is shown. All image processing was done in Fiji (ImageJ) [62, 63] and utilized the ScientiFig Plugin [64] for image overlays.

### Quantification of egg aspect ratio

Ovaries were dissected in freshly made Robb's minimal saline and fixed in Robb's containing 8% EM grade formaldehyde (Polysciences) for 5 min. The tissue was washed 3x in PBT, then disrupted with pipetting to remove the muscle sheath. Tissue was stained with phalloidin (1:200) and DAPI (1 μg/mL, Sigma) for 20 min. Stage 14 egg chambers and mature eggs were mounted and imaged on one of the two scanning confocal microscopes described above, using a 20x/0.8 NA Plan-APOCHROMAT objective. Aspect ratios were calculated by dividing the length of each egg by its width, which were both measured in Fiji (ImageJ) [62, 63]; dorsal appendages were not included in the measurements. To obtain brightfield images of eggs, ovaries were dissected as described above, and eggs were imaged in Robb's media on a Leica MZ FLIII microscope with a Canon Rebel Camera. Image processing was done in Fiji (ImageJ) [62, 63].

### Measurements of global stress fiber alignment

Egg chambers were fixed, stained with phalloidin, and imaged as described above. The orientation of stress fibers in an individual cell was determined by using the Measure function of the OrientationJ plugin [65] for Fiji (ImageJ) [62, 63] after manually selecting a circular region of interest at the basal surface of each cell, excluding cell boundaries. To determine the tissue-level stress fiber alignment (the order parameter) for a given egg chamber, a single imaging plane was used and the orientation of the stress fibers in each cell was compared to all neighboring cells using a custom Python script as previously described [12, 66].

### COMETtail analysis

Flip out clones, as described above, were used to express *UAS-Col4a1-mRFP* in either control or mutant backgrounds. For COMETtail analysis, however, only adult flies were heat shocked (incubated on yeast at 37 °C for 1 h, followed by a 1 h recovery period at 25 °C followed by another hour at 37 °C) and dissected 12 h after the start of the incubation period. Clones were identified by intracellular accumulation of *UAS-Col4a1-mRFP* within the secretory pathway of expressing cells. A COMETtail was scored as being "present" in the BM if it extended more than one cell length away from the clone. Some diffusion can occur even when there is no migration, as was occasionally seen in the *fat2<sup>N103-2</sup>* condition, which is non-migratory [14].

### in vitro binding assay

To test binding between Plexin A and the five *Drosophila* semaphorins, we applied the Extracellular Interactome Assay (ECIA) [72], which is an avidity-based high-throughput interaction detection assay. The ectodomains of PlexA and the five semaphorins were cloned into expression plasmids that produce soluble bait and prey, with an Fc tag for capture on Protein A-coated plates and with a pentamerized Alkaline Phosphatase (AP<sub>5</sub>) tag for detection of binding, respectively. For higher expression levels, the original metallothionein promoter in the ECIA expression plasmids [72, 73] were replaced with the highly active, constitutive Actin5c promoter. The bait and prey were expressed in and secreted from *Drosophila* S2 cells, and the binding of the prey to bait was detected using the BluePhos colorigenic substrate (KPL) for Alkaline Phosphatase with absorbance at 650 nm.

### Quantification of protein localization

Relative levels of Sema-5c-3xGFP and BAC-PlexA-myc at the leading versus trailing edges of cells were quantified in Fiji (ImageJ) [62, 63]. A 10-pixel wide line was drawn along leading-trailing cell-cell interfaces at the basal surface of epithelia that were mosaic for

the tagged protein. The Measure function was then used to obtain an average fluorescence intensity over each line. The leading versus trailing edge of each clone was determined using leading-edge protrusions, which were marked by Phalloidin. Lines were drawn over 3 categories of cell-cell interfaces: leading edges of the clones, trailing edges of the clones, and cell-cell interfaces outside of the clone (background staining). For each epithelium, the intensities from all the measurements within a single category were averaged together to obtain a single value for each epithelium in each category (leading edge, trailing edge, and background); the background level was used to normalize the data. In an individual epithelium, the same number of cell-cell interfaces was quantified across all categories.

*BAC-PlexA-myc* mosaic epithelia were generated by creating Flp FRT clones of *BAC-PlexA-myc* in an epithelium that was null for *PlexA*. It is necessary to use a *PlexA* null background when examining clones of *BAC-PlexA-myc* in order to maintain the endogenous level of *PlexA* in the cells being analyzed (when extra copies of *PlexA* are expressed, its planar polarity is lost). The mosaic tissue was then simultaneously immunostained with anti-*PlexA* and anti-*myc* to boost the signal.

### Quantification of protein colocalization

Line scans were generated by manually drawing a 10-pixel wide line over leading-trailing cell-cell interfaces at the basal epithelial surface using Fiji (ImageJ) [62, 63]. Each line scan spanned 5-8 cells. The PlotProfile function was used to obtain fluorescence intensities for each point along the line, and the data were normalized. Prism (GraphPad) was used to plot them against each other and calculate a Pearson correlation coefficient. *BAC-PlexA-myc* was always used with a *PlexA* deficiency in the background to maintain endogenous levels of *PlexA*, for the reason described above.

### Quantification of protein levels

Levels of *Sema-5c-3xGFP* in *PlexA RNAi* epithelia were quantified at cell-cell interfaces at the basal surface of stage 7 epithelia within a region of uniform size across all samples. Each cell was manually outlined with a 10-pixel wide line in Fiji (ImageJ) [62, 63]; Phalloidin was used to mark cell outlines. The Convert to Mask function was used to create a mask from these outlines. The Multiply function within Image Calculator was then used on the mask and the original image. This creates a new image in which only the pixels contained within the mask are present. The Measure function was used to obtain average fluorescence intensity across the multiplied image and data were normalized.

### Quantification of protrusions

For quantification of protrusion levels, analysis was performed on stage 8 epithelia stained with Phalloidin, as described above. Protrusions were scored by eye and binned into one of three categories based on comparison to controls: normal, weak, or severely depleted. Protrusions were scored as weak if they were reduced in either number or intensity.

For quantification of protrusion orientation, analysis was performed on stage 6 epithelia stained for Phalloidin. A 48 X 38  $\mu\text{m}$  region of the basal surface (approximately 70 cells) was chosen for each sample, and a 10-pixel wide line was manually drawn over all leading-trailing cell-cell interfaces in that region using FIJI (ImageJ) [62, 63]. The average fluorescence intensity along each line was then calculated using the Measure function. For a single epithelium, the measurements from all leading-trailing interfaces were averaged together to generate a single value. Keeping the lines along the leading-trailing interfaces as a guide, a 10-pixel wide line was then manually drawn over all intervening, lateral interfaces. The average fluorescence intensity of these lines was measured and averaged in the same way as the leading-trailing interfaces to produce a single value for a given epithelium. Epithelia whose protrusions were not well preserved through dissection and fixation protocols were excluded from the analysis.

The analysis of protrusion orientation was performed at stage 6 because most *Sema-5c* epithelial are migrating at this stage as shown by COMETtail analysis, which allows a leading-trailing cell interface to be defined by tissue movement. An egg chamber had to have a COMETtail to be included in the analysis. It is important to realize, however, that our quantification method underestimates the extent to which protrusions are mis-oriented in the mutant condition; the measurements along leading-trailing cell-cell interfaces cannot distinguish between a normally oriented protrusion emanating from the leading edge and a mis-oriented protrusion emanating from the trailing edge.

### Generation of *Sema-5c-3xGFP* transgenic line

The *Sema-5c-3xGFP* line was generated by using CRISPR-Cas9 mediated homologous recombination following the general design strategies described by [60, 61]. The target sequence selected for gRNA production was 5'-GTTGCCTAGCGGGTCACGACCGG-3', where the underlined sequence represents the region that was cloned into the pU6-BbsI-chiRNA plasmid, which contains the *Drosophila* snRNA:U6:96Ab promoter for *in vivo* transcription, and the bold sequence represents the adjacent PAM motif.

For homologous recombination, the donor plasmid contained three tandem copies of GFP coding sequence followed by a floxed 3xP3-DsRed module [61] for screening insertion events. This entire cassette was flanked by approximately 2 kb homology arms that contained sequence that matched either side of the target locus. The insertion was made after position 13,696 in the *Sema-5c* gene, immediately before the stop codon, which corresponds to amino acid 1093 of the *Sema-5c* protein (according to isoform A sequence).

Injections were performed by Genetivision Inc. into transgenic embryos expressing Cas9 under the *nanos* promoter. Resulting adults were mated to balancer flies and progeny were screened for founders using DsRed expression in the adult eye with a Leica

MZ FL III microscope. Founders were used to establish stocks and crossed to *Cre*-expressing flies to excise the DsRed module. Insertions were verified by sequencing. Two independent lines were derived and no differences were observed between them.

#### **Generation of UAS-Sema-5c-GFP transgenic line**

Sema5c full-length cDNA without a stop codon was amplified from clone RE68041 and inserted into pENTR/D-TOPO and then transferred to the *Drosophila* Gateway Collection vector pTWG for C-terminal GFP tagging. *UAS-Sema5c-GFP* flies were generated using P element injection by GenetiVision. Insertions were verified by sequencing. Two independent lines were derived and no differences were observed between them.

#### **QUANTIFICATION AND STATISTICAL ANALYSIS**

All data were obtained from at least two independent experiments, and several females were analyzed each time. All data were highly reproducible. No statistical method was used to predetermine sample size. The sample size for each experiment can be found in the figure panel or in the figure legend. A Student's t test was used to determine if two datasets were significantly different. This analysis was performed using Prism software, version 6 (GraphPad). These tests are appropriate because all data obtained follow an approximately normal distribution. These experiments were not randomized, nor was the data analysis performed blind. Egg chambers damaged by the dissection process were not included in the analysis.

Current Biology, Volume 29

## Supplemental Information

**Planar-Polarized Semaphorin-5c and Plexin A**

**Promote the Collective Migration**

**of Epithelial Cells in *Drosophila***

**Claire G. Stedden, William Menegas, Allison L. Zajac, Audrey M. Williams, Shouqiang Cheng, Engin Özkan, and Sally Horne-Badovinac**

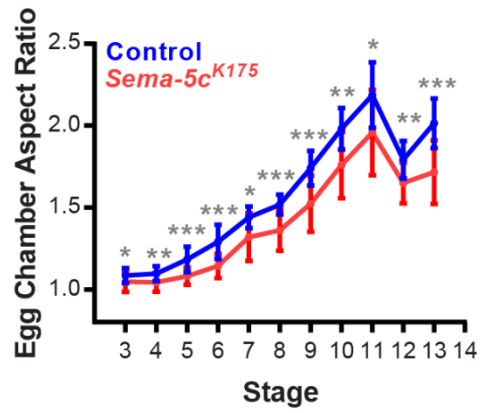
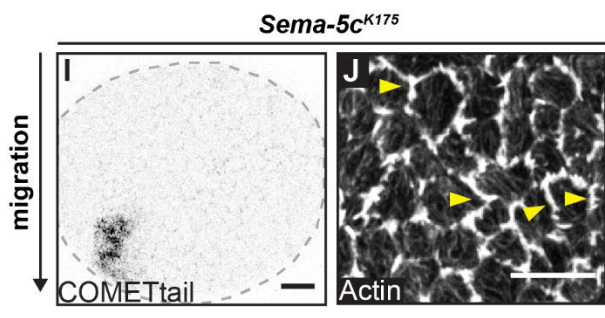
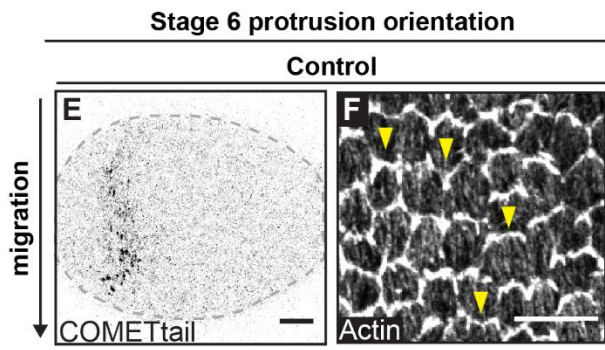
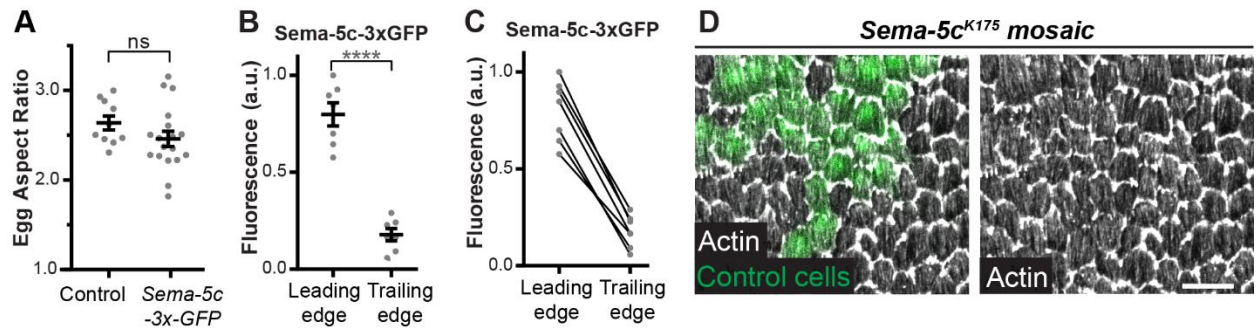


**Figure S1. Further analysis of Sema-5c's role in egg chamber elongation, related to Figure 1**

Quantification of egg chamber aspect ratios. Egg chambers from *Sema-5c<sup>K175</sup>* females are rounder than controls.  $n \geq 10$  for all conditions.

Data represent mean  $\pm$  SEM. Unpaired t-test. \* $p < 0.05$ ; \*\* $p < 0.01$ ; \*\*\* $p < 0.001$ .



**Actin levels along cell-cell interfaces**

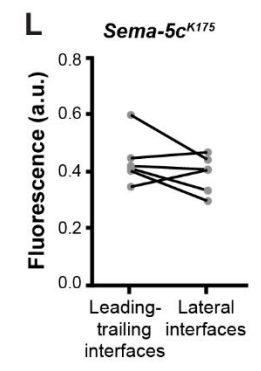
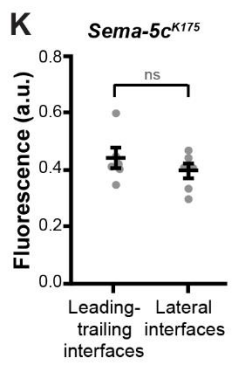
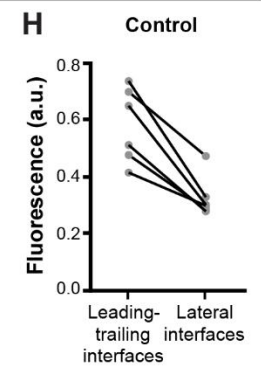
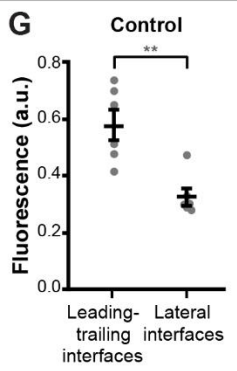


**Figure S2. Characterization of Sema-5c-3xGFP and effect of Sema-5c loss of function on protrusions, related to Figure 4**

(A) Quantification of egg aspect ratios. The 3xGFP tag on Sema-5c does not cause a defect in egg shape.

(B and C) Quantification of fluorescence intensity of Sema-5c-3xGFP at leading versus trailing edges of *Sema-5c-3xGFP* clones, stage 7. Each data point is one epithelium in which line scans were performed along 3-8 leading or trailing cell-cell interfaces. (B) The first graph shows the data for statistical purposes. (C) The second graph links the leading and trailing measurements for each egg chamber with a line.

(D) Images of the basal surface of a *Sema-5c*<sup>K175</sup> mosaic epithelium, stage 7. Loss of Sema-5c has no obvious effect on cellular protrusions at this stage.

(E and F) Images of the basal surface of a wild-type egg chamber. (E) The COMETtail image shows that the epithelium was migrating prior to fixation. (F) The image showing the actin cytoskeleton at the basal surface is from the same egg chamber. The protrusions are primarily oriented in the direction of migration (closed triangles).

(G and H) Quantification of protrusion orientation along opposing cell-cell interfaces in wild-type epithelia (see STAR methods). Because actin levels are particularly high in protrusions, actin levels can be used as a proxy for protrusion position. (G) The first graph shows the data for statistical purposes. (H) The second graph links the two measurements for each egg chamber with a line.

(I and J) Images of the basal surface of a *Sema-5c* egg chamber. (I) The COMETtail image shows that the epithelium was migrating prior to fixation. (J) The image showing the actin cytoskeleton at the basal surface is from the same egg chamber. The protrusions are often oriented away from the direction of migration (open triangles).

(K and L) Quantification of protrusion orientation along opposing cell-cell interfaces in *Sema-5c* epithelia (see STAR methods). Because actin levels are particularly high in protrusions, actin levels can be used as a proxy for protrusion position. (K) The first graph shows the data for statistical purposes. (L) The second graph links the two measurements for each egg chamber with a line.

Data represent mean  $\pm$  SEM. Unpaired t-test. ns, not significant ( $p > 0.05$ ), \*\*  $p < 0.01$ , \*\*\*\* $p < 0.0001$ . Scale bars, 10  $\mu\text{m}$  (D-F, I and J).

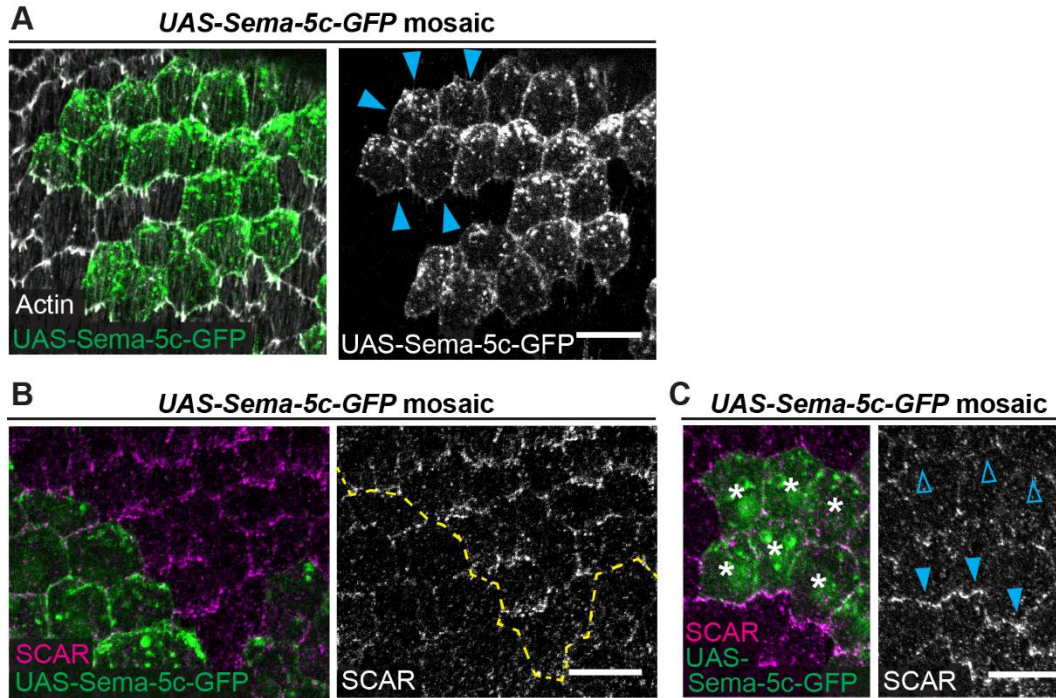


**Figure S3. Effect of Sema-5c overexpression on protrusions, related to Figure 4**

(A) Images of the basal surface of a *UAS-Sema-5c-GFP* mosaic epithelium, stage 7. Sema-5c localizes all around the plasma membrane when overexpressed (blue triangles).

(B and C) Images of the basal surface of *UAS-Sema-5c-GFP* mosaic epithelia with SCAR immunostaining, stage 7. (B) The larger clone shows that SCAR is reduced when *Sema-5c* is overexpressed. Dashed line marks the clone boundary. (C) The smaller clone (asterisks) shows that SCAR is lost from the leading edge of cells directly behind *Sema-5c* overexpressing cells (open triangles), but not from the leading edge of the *Sema-5c* overexpressing cells themselves (closed triangles).

Scale bars, 10  $\mu$ m.

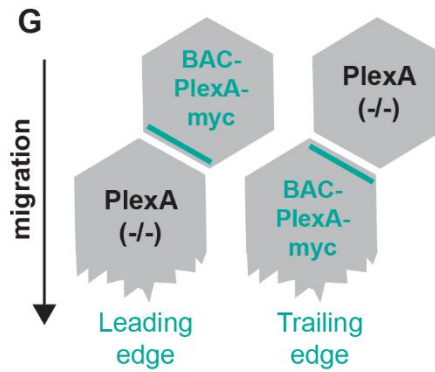
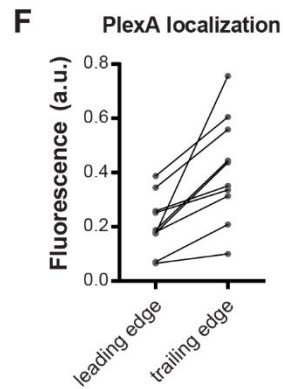
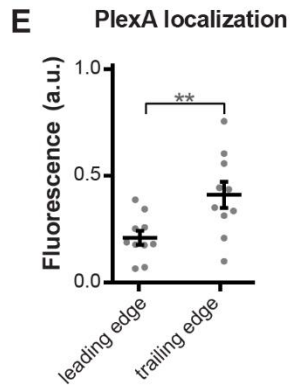
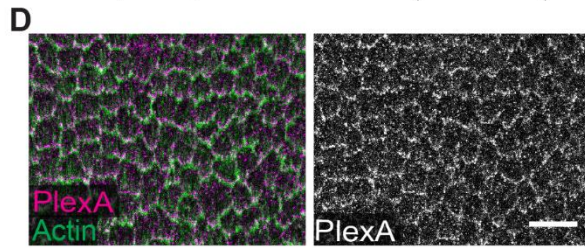
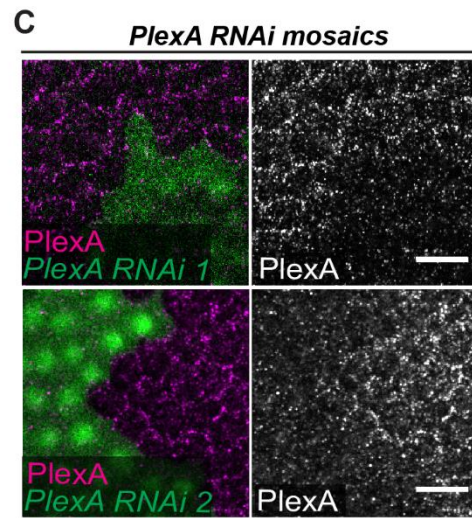
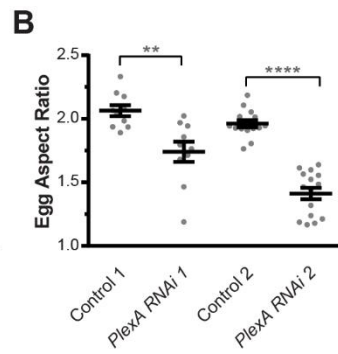
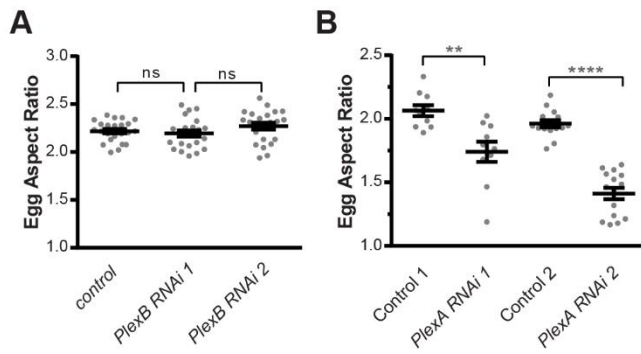


#### Figure S4. Analysis of Plexin reagents and PlexA localization, related to Figure 5

(A) Quantification of egg aspect ratios. Expressing either of two previously validated *PlexB RNAi* transgenes in the follicular epithelium fails to affect egg shape.

(B) Quantification of egg aspect ratios. Expressing either of two independent *PlexA RNAi* transgenes in the follicular epithelium results in eggs that are rounder than controls.

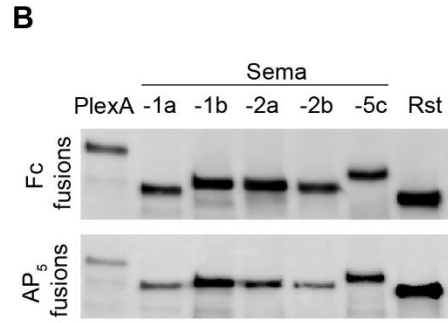
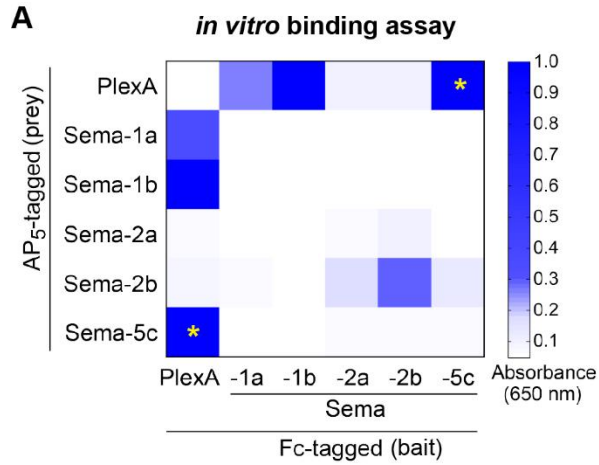
(C) Images of the basal surface of *PlexA RNAi* mosaic epithelia, stage 7. PlexA immunostaining is reduced by two independent *PlexA RNAi* transgenes.

(D) Image of PlexA immunostaining at the basal epithelial surface, stage 7. PlexA is punctate along leading-trailing cell-cell interfaces.

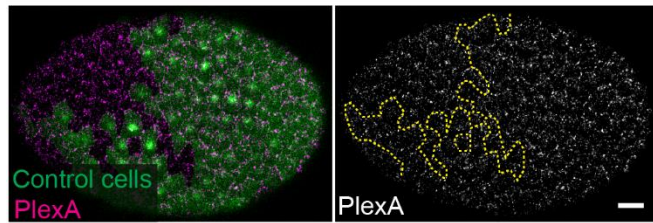
(E and F) Quantification of fluorescence intensity of BAC-PlexA-myc, anti-myc and anti-PlexA immunostaining, at leading versus trailing interfaces of *BAC-PlexA-myc* clones in a *PlexA* null background, stage 7. Each point is one epithelium in which line scans were performed along 6-15 leading or trailing cell-cell interfaces. (E) The first graph shows the data for statistical purposes. (F) The second graph links the leading and trailing measurements for each egg chamber with a line.

(G) Illustration depicting the populations of BAC-PlexA-myc quantified in (E and F).

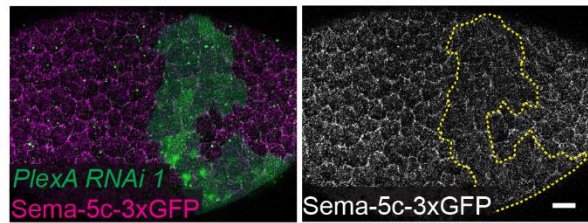
Data represent mean  $\pm$  SEM. Unpaired t-test. ns, not significant ( $p > 0.05$ ), \*\* $p < 0.01$ ; \*\*\*\* $p < 0.0001$ . Scale bars, 10  $\mu\text{m}$ .



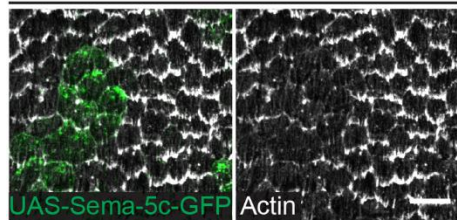
**C** *Sema-5c*<sup>K175</sup> mosaic



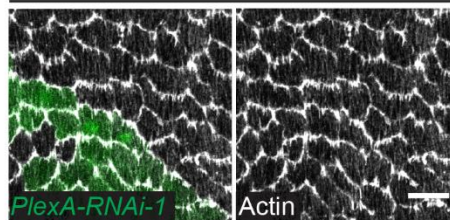
**D** *PlexA RNAi 1* mosaic



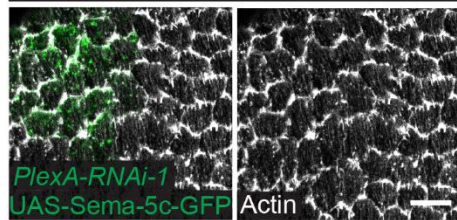
**E** *UAS-Sema-5c-GFP* mosaic



**F** *PlexA-RNAi-1* mosaic



**G** *UAS-Sema-5c-GFP* & *PlexA-RNAi-1* mosaic



**H** Protrusions in:

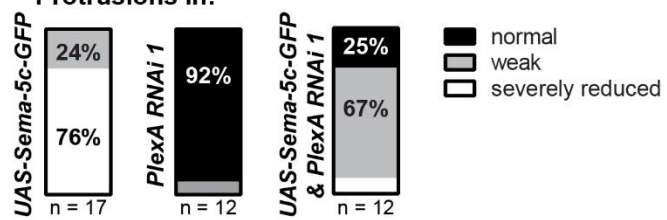


### Figure S5. Further investigation of Sema-5c – PlexA interactions, related to Figure 6

(A) Interaction grid for the binding between the PlexA ectodomain and the ectodomains of the five *Drosophila* semaphorins. Binding of prey to bait was detected using the BluePhos colorigenic substrate (KPL) for Alkaline Phosphatase (see STAR Methods). Sema-1a and Sema-1b are PlexA ligands and thus serve as positive controls. Sema-2a and Sema-2b are PlexB ligands and serve as negative controls. The yellow asterisks highlight strong binding between PlexA and Sema-5c. The binding seen between some of the Sema ligands was unexpected, but may be consistent with a previous report of a possible Sema-1a - Sema-2a interaction [S1].

(B) Western blot showing the expression levels of the ectodomains used in (A), Roughest (Rst) was used as a positive control.

(C) Image of PlexA immunostaining at the basal surface of a *Sema-5c*<sup>K175</sup> mosaic epithelium, stage 7. PlexA levels are not affected by loss of Sema-5c.

(D) Image of the basal surface of a *PlexA RNAi* mosaic epithelium, stage 7. *PlexA RNAi* cells pseudocolored green. Sema-5c-3XGFP levels are reduced by loss of PlexA.

(E-G) Depletion of PlexA abrogates Sema-5c's ability to suppress protrusions. Images of the basal epithelial surface, stage 8. (E) Clones of cells expressing *UAS-Sema-5c-GFP* have strongly reduced protrusions. (F) Clones of cells expressing *UAS-PlexA-RNAi* have largely normal protrusions. (G) Co-expressing *UAS-PlexA-RNAi* with *UAS-Sema-5c-GFP* partially rescues the protrusion defect induced by *Sema-5c* overexpression.

(H) Quantification of the data presented in (E-G). n = number of egg chambers examined.

Scale bars, 10  $\mu$ m.

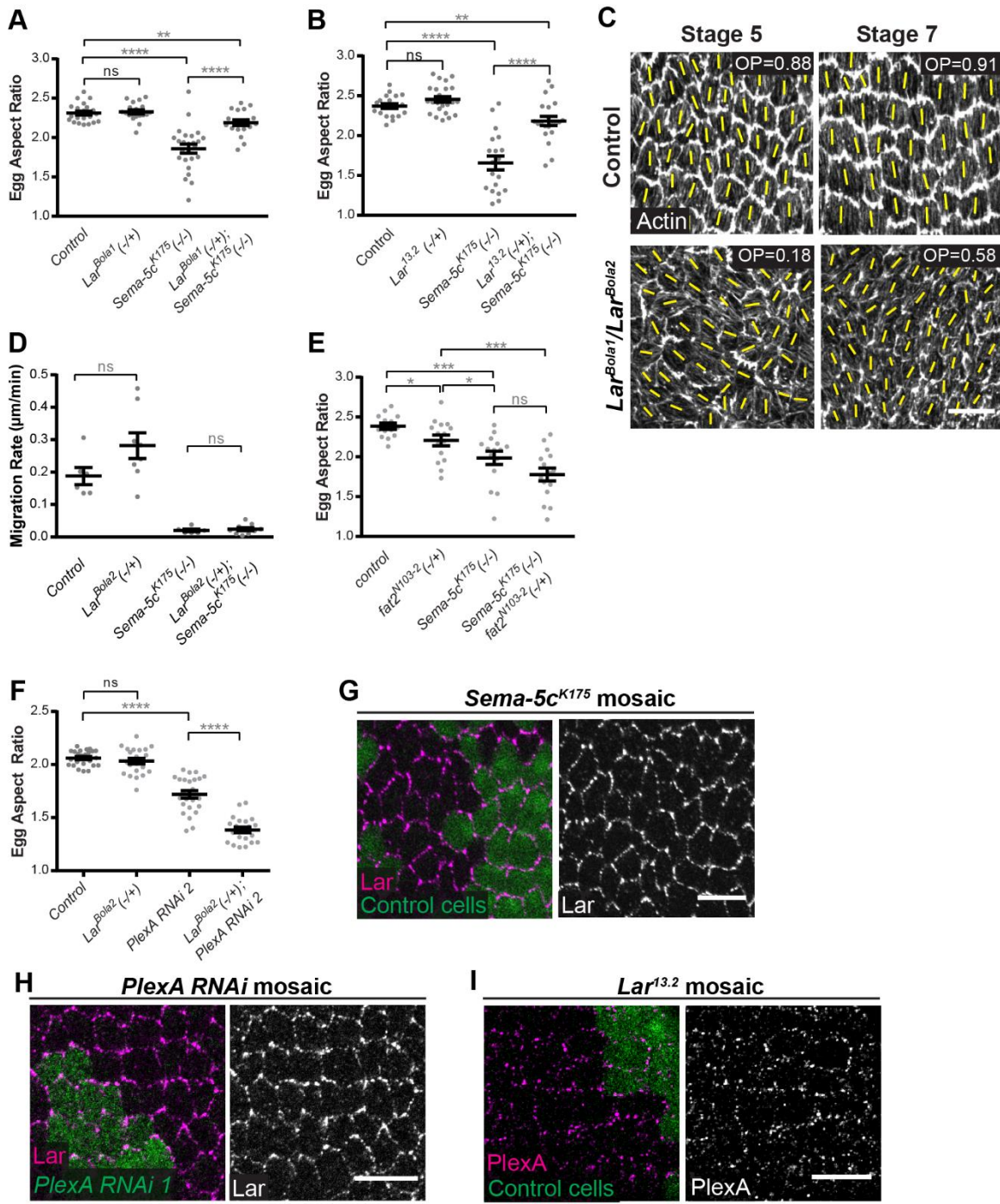


**Figure S6. Investigating the interaction between Sema-5c, PlexA, Lar, and Fat2, related to Figure 7**

(A and B) Quantification of egg aspect ratios. Removing one copy of *Lar* largely rescues the egg shape defect in *Sema-5c*<sup>K175</sup> females. Data are shown for two independent alleles of *Lar*.

(C) Images of global stress fiber alignment for the control and *Lar*<sup>Bola</sup>/*Lar*<sup>Bola2</sup> conditions analyzed in Figures 6B and 6C. Yellow lines show the primary stress fiber direction in each cell. OP = order parameter.

(D) Quantification of migration rates. Removing one copy of *Lar* in the *Sema-5c*<sup>K175</sup> background does not rescue the migration rate, stage 7.

(E and F) Quantification of egg aspect ratios. Elongation is neither rescued by loss of one copy of *fat2* in a *Sema-5c*<sup>K175</sup> background (E), nor by loss of one copy of *Lar* in a *PlexA RNAi* background (F).

(G) Image of Lar immunostaining at the basal surface of a *Sema-5c*<sup>K175</sup> mosaic epithelium, stage 7. Lar levels are not affected by loss of Sema-5c.

(H) Image of Lar immunostaining at the basal surface of a *PlexA RNAi* mosaic epithelium, stage 7. Lar levels are not affected by loss of PlexA.

(I) Image of PlexA immunostaining at the basal surface of a *Lar*<sup>13.2</sup> mosaic epithelium, stage 7. PlexA levels are not affected by loss of Lar.

Data represent mean ± SEM. Unpaired t-test. ns, not significant ( $p > 0.05$ ), \* $p < 0.05$ ; \*\* $p < 0.01$ ; \*\*\* $p < 0.001$ ; \*\*\*\* $p < 0.0001$ . Scale bars, 10  $\mu\text{m}$ .

Figure	Panel	Genotype
1	D	w;; <i>FRT80B</i>
		w;; <i>Sema-5c<sup>K175</sup></i> , <i>FRT80B</i>
	E	w;; <i>FRT80B</i>
		w;; <i>Sema-5c<sup>K175</sup></i> , <i>FRT80B</i>
	w;; <i>Df(3L)BSC840/+</i>	
	w;; <i>Df(3L)BSC840/Sema-5c<sup>K175</sup></i> , <i>FRT80B</i>	
2	A-D	w;; <i>FRT80B</i>
		w;; <i>Sema-5c<sup>K175</sup></i> , <i>FRT80B</i>
3	A-E, J	<i>hsFlp/w; UAS-Col4a1-RFP/act5c&gt;&gt;Gal4, UAS-GFP</i>
	F, G, J	<i>hsFlp/w; UAS-Col4a1-RFP/act5c&gt;&gt;Gal4, UAS-GFP; fat2<sup>N103-2</sup>, FRT80B</i>
	H-J	<i>hsFlp/w; UAS-Col4a1-mRFP/act5c&gt;&gt;Gal4, UAS-GFP; Sema-5c<sup>K175</sup>, FRT80B</i>
4	A-F	w;; <i>Sema-5c-3xGFP</i>
	G-I	w/+; <i>e22cc-Gal4, UAS-Flp/+; Sema-5c-3xGFP, FRT80B/FRT80B</i>
	J	<i>hsFlp/w; act5c&gt;&gt;gal4/+; UAS-Sema-5c-GFP/+</i>
	K	<i>hsFlp/w;; act5c&gt;&gt;gal4, UAS-RFP/UAS-Sema-5c-GFP</i>
5	A	w; <i>traffic jam-Gal4/+</i>
		w; <i>traffic jam-Gal4/UAS-PlexA RNAi<sup>GD14483</sup></i>
	B-D	w; <i>traffic jam-Gal4/+; UAS-Dicer-2/+</i>
		w/ y, sc, v <sup>1</sup> ; <i>traffic jam-Gal4/+; UAS-PlexA RNAi<sup>TRiP.HM05221</sup>/UAS-Dicer-2</i>
E	w;; <i>BAC-PlexA-myc/+; Df(4)C3/+</i>	
F-H	<i>yw hsFlp;; BAC-PlexA-myc, ubiGFP, h, FRT80B/FRT80B, e ca; Df(4)C3/PlexA<sup>MB09499</sup></i>	
6	A-B	w; <i>traffic jam-Gal4/+; Sema-5c-3xGFP/+</i>
		w; <i>traffic jam-Gal4/ UAS-PlexA RNAi<sup>GD14483</sup>; Sema-5c-3xGFP/+</i>
	C-G	w;; <i>BAC-PlexA-myc, Sema-5c-3xGFP/+; Df(4)C3/+</i>
	H-K	w; <i>traffic jam-Gal4/UAS-RFP-RNAi; UAS-Sema-5c-GFP/+</i>
w; <i>traffic jam-Gal4/UAS-HA-PlexA</i>		
	w; <i>traffic jam-Gal4/UAS-HA-PlexA; UAS-Sema-5c-GFP/+</i>	
7	A-D	w <sup>1118</sup>
		w/+; <i>Lar<sup>Bola2</sup>/+</i>
		<i>Lar<sup>Bola1</sup>/Lar<sup>Bola2</sup></i>
		w;; <i>Sema-5c<sup>K175</sup></i> , <i>FRT80B</i>
	w; <i>Lar<sup>Bola2</sup>/+; Sema-5c<sup>K175</sup>, FRT80B</i>	
E-I	w;; <i>Sema-5c-3xGFP</i>	

	J	<i>w; Lar<sup>13.2</sup>, FRT40A /ubi-mRFP, FRT40A; Sema5c-3xGFP /T155-Gal4, UAS-Flp</i>
S1		<i>w;; FRT80B</i>
		<i>w;; Sema-5c<sup>K175</sup>, FRT80B</i>
S2	A	<i>w</i>
		<i>w;; Sema-5c-3xGFP</i>
	B-C	<i>w/+; e22cc-Gal4, UAS-Flp/+; Sema-5c-3xGFP, FRT80B/FRT80B</i>
	D	<i>w/+; e22cc-Gal4, UAS-Flp/+; Sema-5c<sup>K175</sup>, FRT80B/ubi-eGFP, FRT80B</i>
	E-H	<i>hsFlp/ w; UAS-Col4a1-mRFP/act5c&gt;&gt;Gal4, UAS-GFP</i>
	I-L	<i>hsFlp/ w; UAS-Col4a1-mRFP/act5c&gt;&gt;Gal4, UAS-GFP; Sema-5c<sup>K175</sup>, FRT80B</i>
S3	A	<i>hsFlp/w; UAS-Sema-5c-GFP/+; act5c&gt;&gt;Gal4/+</i>
	B-C	<i>hsFlp/w; act5c&gt;&gt;Gal4, UAS-GFP/+; UAS-Sema-5c-GFP/+</i>
S4	A	<i>w; traffic jam-Gal4/+; UAS-Dicer-2/+</i>
		<i>w; traffic jam-Gal4/+; UAS-Dicer-2/UAS-PlexB RNAi<sup>GD14473</sup></i>
		<i>w; traffic jam-Gal4/UAS-PlexB RNAi<sup>GD1350</sup>; UAS-Dicer-2/+</i>
	B	<i>w; traffic jam-Gal4/+</i>
		<i>w; traffic jam-Gal4/UAS-PlexA RNAi<sup>GD14483</sup></i>
		<i>w; traffic jam-Gal4/+; UAS-Dicer-2/+</i>
		<i>w/y, sc, v<sup>1</sup>; traffic jam-Gal4/+; UAS-PlexA RNAi<sup>TRiP.HM05221</sup>/UAS-Dicer-2</i>
	C	<i>hsFlp/w; UAS-PlexA RNAi<sup>GD14483</sup>/+; act5c&gt;&gt;Gal4, UAS-GFP/+</i>
		<i>hsFlp/ y, sc, v<sup>1</sup>; UAS-Dicer-2/+; UAS-PlexA RNAi<sup>TRiP.HM05221</sup>/act5c&gt;&gt;Gal4, UAS-GFP</i>
	D	<i>w<sup>1118</sup></i>
E-F	<i>yw hsFlp;; BAC-PlexA-myc, ubiGFP, h, FRT80B/FRT80B, e ca; Df(4)C3/PlexA<sup>MB09499</sup></i>	
S5	C	<i>w; e22cc-Gal4, UAS-Flp/+; Sema-5c<sup>K175</sup>, FRT80B/ubi-eGFP, FRT80B</i>
	D	<i>hsFlp/w; UAS-PlexA RNAi<sup>GD14483</sup>/act5c&gt;&gt;Gal4, UAS-LacZ; Sema-5c-3xGFP/+</i>
	E-H	<i>hsFlp/w; act5c&gt;&gt;Gal4, UAS-LacZ/+; UAS-Sema-5c-GFP/+</i>
		<i>hsFlp/w; act5c&gt;&gt;Gal4, UAS-GFP/UAS-PlexA RNAi<sup>GD14483</sup></i>
	<i>hsFlp/w; UAS-PlexA RNAi<sup>GD14483</sup>/+; UAS-Sema-5c-GFP/act5c&gt;&gt;Gal4</i>	
S6	A	<i>w<sup>1118</sup></i>
		<i>w<sup>1118</sup>/+; Lar<sup>Bola1</sup>/+</i>
		<i>w;; Sema-5c<sup>K175</sup>, FRT80B</i>
		<i>w; Lar<sup>Bola1</sup>/+; Sema-5c<sup>K175</sup>, FRT80B</i>
	B	<i>w<sup>1118</sup></i>
		<i>w<sup>1118</sup>/+; Lar<sup>13.2</sup> FRT40A/+</i>

		<i>w</i> ;; <i>Sema-5c</i> <sup>K175</sup> , <i>FRT80B</i>
		<i>w</i> ; <i>Lar</i> <sup>13.2</sup> <i>FRT40A/+</i> ; <i>Sema-5c</i> <sup>K175</sup> , <i>FRT80B</i>
	C	<i>w</i> <sup>1118</sup>
		<i>Lar</i> <sup>Bola1</sup> / <i>Lar</i> <sup>Bola2</sup>
	D	<i>w</i> <sup>1118</sup>
		<i>w/+</i> ; <i>Lar</i> <sup>Bola2</sup> / <i>+</i>
		<i>w</i> ;; <i>Sema-5c</i> <sup>K175</sup> , <i>FRT80B</i>
		<i>w</i> ; <i>Lar</i> <sup>Bola2</sup> / <i>+</i> ; <i>Sema-5c</i> <sup>K175</sup> , <i>FRT80B</i>
	E	<i>w</i> <sup>1118</sup>
		<i>w</i> ;; <i>fat2</i> <sup>N103.2</sup> , <i>FRT80B/+</i>
		<i>w</i> ;; <i>Sema-5c</i> <sup>K175</sup> , <i>FRT80B</i>
		<i>w</i> ; <i>fat2</i> <sup>N103.2</sup> , <i>Sema-5c</i> <sup>K175</sup> / <i>Sema-5c</i> <sup>K175</sup> , <i>FRT80B</i>
	F	<i>w</i> ; <i>traffic jam-Gal4/+</i> ; <i>UAS-Dicer-2/+</i>
		<i>w</i> ; <i>traffic jam-Gal4/Lar</i> <sup>Bola2</sup> ; <i>UAS-Dicer-2/+</i>
		<i>w/ y, sc, v</i> <sup>1</sup> ; <i>traffic jam-Gal4/+</i> ; <i>UAS-Dicer-2/UAS-PlexA RNAi</i> <sup>TRIP.HM05221</sup>
		<i>w</i> ; <i>traffic jam-Gal4/Lar</i> <sup>Bola2</sup> ; <i>UAS-Dicer-2/UAS-PlexA RNAi</i> <sup>TRIP.HM05221</sup>
	G	<i>w</i> ; <i>e22cc-Gal4, UAS-Flp/+</i> ; <i>Sema-5c</i> <sup>K175</sup> , <i>FRT80B/Ubi-eGFP, FRT80B</i>
	H	<i>hsFlp/w</i> ; <i>UAS-PlexA RNAi</i> <sup>GD14483</sup> / <i>+</i> ; <i>act5c&gt;&gt;Gal4, UAS-GFP/+</i>
	I	<i>w</i> ; <i>ubi-mRFP, FRT40A/Lar</i> <sup>13.2</sup> , <i>FRT40A</i> ; <i>T155-Gal4, UAS-Flp/+</i>
Video	S1	<i>w</i> ;; <i>FRT80B</i>
		<i>w</i> ;; <i>Sema-5c</i> <sup>K175</sup> , <i>FRT80B</i>
Video	S2	<i>w</i> ; <i>traffic jam-Gal4/+</i> ; <i>UAS-Dicer-2/+</i>
		<i>w/ y, sc, v</i> <sup>1</sup> ; <i>traffic jam-Gal4/+</i> ; <i>UAS-PlexA RNAi</i> <sup>TRIP.HM05221</sup> / <i>UAS-Dicer-2</i>

**Table S1. Experimental Genotypes, Related to STAR Methods**

Figure	Panel	Females on yeast		
		Adult age (days)	Temp (°C)	Duration (days)
1	D-E	1-2	25	2
2	A-D	1-2	25	2
3	A-E	1-2	25 (post heat shock)	0.5
4	A-F	1-2	25	2
	G-I	1-3	29	3
	J-K'	1-2	29 (post heat shock)	1
5	A-D	1-3	29	3
	E	1-2	25	2
	F-H	1-2	25 (post heat shock)	2
6	A-B	1-2	29	3
	C-G	1-2	25	2
	H-K	1-2	29	2
7	A-I	1-2	25	2
	J	1-3	25	2
S1	A	1-2	25	2
S2	A	1-2	25	2
	B-C	1-3	29	3
	D	1-3	29	3
	E-L	1-2	25 (post heat shock)	0.5
S3	A	1-2	29 (post heat shock)	2
	B-C	1-2	29 (post heat shock)	1
S4	A-B	1-3	29	3
	C	1-2	29 (post heat shock)	1
	D	1-2	25	2
	E-F	1-2	25 (post heat shock)	2
S5	C	1-2	29	3
	D	1-2	29 (post heat shock)	1
	E-H	1-2	29 (post heat shock)	1.5
S6	A-E	1-2	25	2
	F	1-3	29	3
	G	1-2	29	3
	H	1-2	29 (post heat shock)	1
	I	1-3	29	4
Video	S1	2	25	2
Video	S2	1-3	29	3

**Table S2. Conditions for the culturing of experimental females, Related to STAR methods**

## **SUPPLEMENTAL REFERENCES**

- S1. Sweeney, L.B., Chou, Y.-H., Wu, Z., Joo, W., Komiyama, T., Potter, C.J., Kolodkin, A.L., Garcia, K.C., and Luo, L. (2011). Secreted Semaphorins from Degenerating Larval ORN Axons Direct Adult Projection Neuron Dendrite Targeting. *Neuron* 72, 734–747.